CENTER FOR CONNECTED AND AUTOMATED TRANSPORTATION

Final Report #24
December 2022

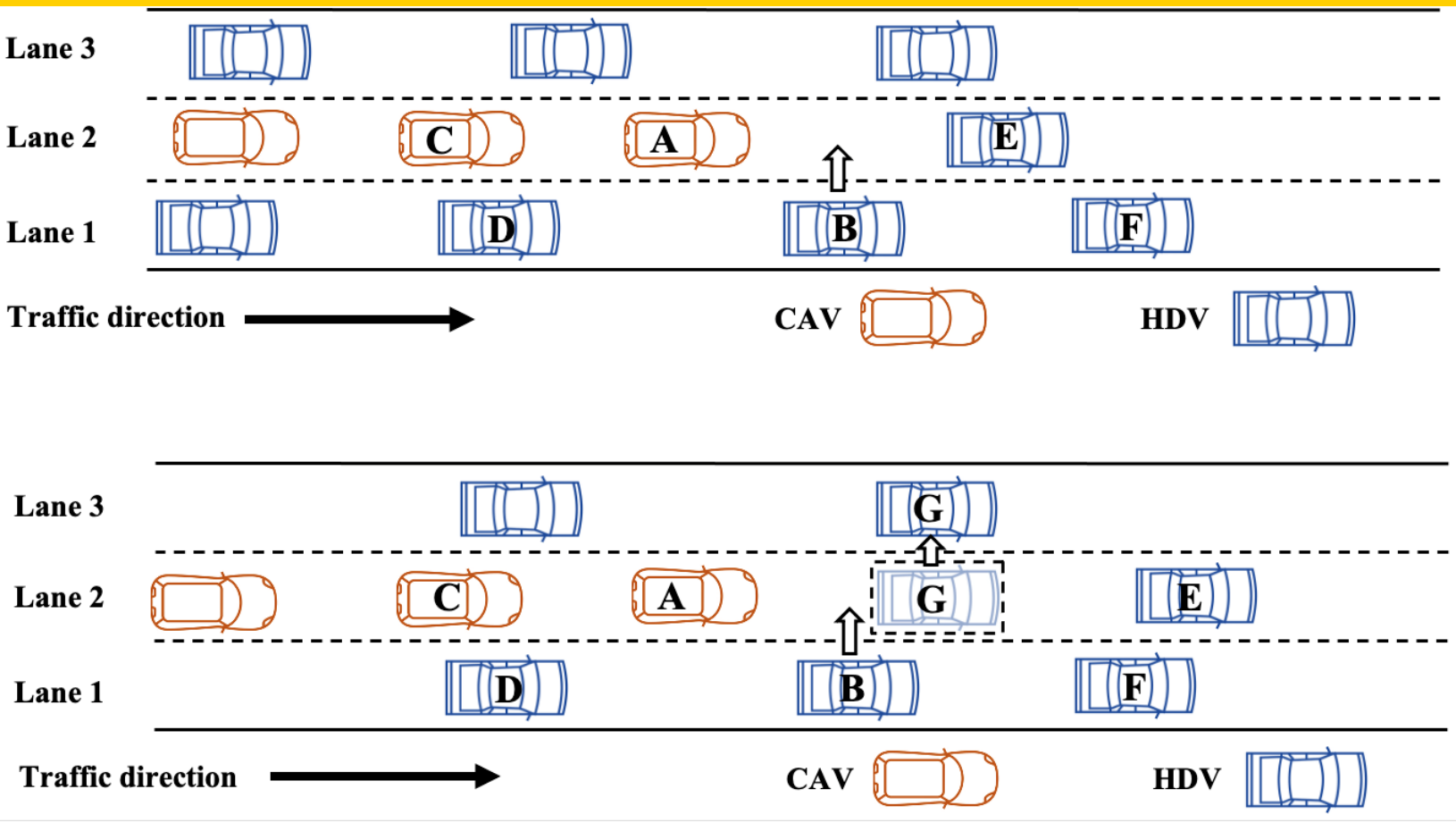

Non-connected Vehicle Detection Using Connected Vehicles

Yongyang Liu
Anye Zhou
Yu Wang
Srinivas Peeta

PURDUE UNIVERSITY

CENTER FOR CONNECTED AND AUTOMATED TRANSPORTATION

Report No. 24
Project Start Date: 1/1/2018
Project End Date: 12/31/2022

Report Date: December 2022

Non-connected vehicle detection using connected vehicles

Yongyang Liu

Graduate Researcher
Georgia Institute of Technology

Anye Zhou

Graduate Researcher
Georgia Institute of Technology

Yu Wang

Postdoctoral Fellow
Georgia Institute of Technology

Srinivas Peeta

Frederick R. Dickerson Chair & Professor
Georgia Institute of Technology

UMTRI | The University of Akron | Illinois Center for Transportation | Purdue University | Washtenaw Community College | Central State University

ACKNOWLEDGEMENTS AND DISCLAIMER

Funding for this research was provided by the Center for Connected and Automated Transportation under Grant No. 69A3551747105 of the U.S. Department of Transportation, Office of the Assistant Secretary for Research and Technology (OST-R), University Transportation Centers Program. The work was carried out by researchers at the Georgia Institute of Technology through a subcontract with Purdue University. The contents of this report reflect the views of the authors, who are responsible for the facts and the accuracy of the information presented herein. This document is disseminated under the sponsorship of the Department of Transportation, University Transportation Centers Program, in the interest of information exchange. The U.S. Government assumes no liability for the contents or use thereof.

Suggested APA Format Citation:

Liu, Y., Zhou, A., Wang, Y., Peeta, S. (2022). Non-Connected Vehicle Detection Using Connected Vehicles, Technical Report Nr. 24, Center for Connected and Automated Transportation, Purdue University, West Lafayette, IN.

Contact Information

Samuel Labi
Purdue University
3000 Kent Ave, West Lafayette, IN
Phone: (765) 494-5926
Email: labi@purdue.edu

Srinivas Peeta
Georgia Institute of Technology
788 Atlantic Dr, Atlanta, GA
Phone: (404) 894-2243
Email: peeta@gatech.edu

CCAT
University of Michigan Transportation Research Institute
2901 Baxter Road
Ann Arbor, MI 48152

uumtri-ccat@umich.edu
(734) 763-2498
www.ccat.umtri.umich.edu

Technical Report Documentation Page

1. Report No. CCAT Report #24	**2. Government Accession No.** N/A	**3. Recipient's Catalog No.** N/A
4. Title and Subtitle Non-connected vehicle detection using connected vehicles		**5. Report Date** December 2022 **6. Performing Organization Code** N/A
7. Author(s) Yongyang Liu, Anye Zhou, Yu Wang, Srinivas Peeta		**8. Performing Organization Report No.** N/A
9. Performing Organization Name and Address Center for Connected and Automated Transportation Purdue University, 550 Stadium Mall Drive, W. Lafayette, IN 47907; and University of Michigan Ann Arbor, 2901 Baxter Rd, Ann Arbor, MI 48109		**10. Work Unit No.** N/A **11. Contract or Grant No.** Contract No. 69A3551747105
12. Sponsoring Agency Name and Address U.S. Department of Transportation Office of the Assistant Secretary for Research and Technology 1200 New Jersey Avenue, SE Washington, DC 20590		**13. Type of Report and Period Covered:** Final Report, 1/1/2018 to 12/31/2022 **14. Sponsoring Agency Code** OST-R
15. Supplementary Notes Conducted under the U.S. DOT Office of the Assistant Secretary for Research and Technology's (OST-R) University Transportation Centers (UTC) program.		

16. Abstract

Connected vehicle (CV) technologies are entering the realm of deployment. They have the potential to help drivers make safe, reliable, and informed decisions, and thereby to enhance network capacity and reduce congestion. During the transition to CV technologies, there will be mixed-flow traffic streams of CVs and non-CVs, i.e., human-driven vehicles (HDVs). While most studies have analyzed the CV car-following behavior in a pure CV environment, there is the need for a comprehensive CV car-following model in general mixed flow environment. Specifically, mixed-flow traffic introduces key challenges for CV operations due to potential lane changes by HDVs in adjacent lanes, which can cause stop-and-go waves and traffic oscillations. An understanding of the interactions between CVs and HDVs in the lane-change process can be leveraged to enhance the CV platoon operations. This study proposes a deep reinforcement learning-based proactive longitudinal control strategy (PLCS) for CVs to counteract disruptive HDV lane-change behaviors that can induce disturbances, and to preserve the smoothness of traffic flow in the CV platooning control process. In it, a Transformer-based lane-change traffic condition predictor is constructed to predict longitudinal trajectories of HDVs and whether an HDV will likely perform a disruptive lane change under the ambient traffic conditions. If no disruptive lane change is predicted, an extended intelligent driver model is activated for the CV to perform smooth car-following behavior under cooperative CV platooning control. If a disruptive lane change is predicted, a rainbow deep Q-Network (RDQN)-based lane-change preclusion model is proposed through which the CV can alter the lane-change traffic condition to preclude the HDV's lane change. Results from numerical experiments suggest that a CV controlled by the PLCS is effective in reducing disruptive lane-change maneuvers by an HDV in its vicinity and can improve string stability performance in mixed-flow traffic. Further, the effectiveness of the PLCS is illustrated under different lane-change scenarios, CV control setups, and HDV driver types.

17. Key Words Connected vehicles, Car following, Trajectory prediction, Mixed-flow traffic		**18. Distribution Statement** No restrictions.	
19. Security Classif. (of this report) Unclassified	**20. Security Classif. (of this page)** Unclassified	**21. No. of Pages** 46 pages	**22. Price** N/A

Form DOT F 1700.7 (8-72) Reproduction of completed page authorized

Table of Contents

LIST OF FIGURES

LIST OF TABLES

1. INTRODUCTION

Connected vehicle (CV) technology has the potential to help drivers and vehicles make safe, reliable, and informed decisions, thereby enabling network capacity optimization and congestion reduction. By using kinematic information obtained through vehicle-to-vehicle (V2V) communications, CVs can transmit kinematic state (i.e., spacing, speed, and acceleration) information to each other. Such information can improve drivers' situational awareness and aid them to adjust driving behavior in relation to preceding vehicles. With appropriate human-machine interface (HMI) and Advanced Driver Assistance Systems (ADAS) to supply this information, CVs can develop cooperative driving strategies to enhance safety, attenuate propagation of traffic shockwaves (Jia et al., 2016; Zhou et al., 2020), and improve link capacity (Shladover et al., 2012; van Arem et al., 2006). This study implemented a cooperative driving strategy in the sense of Cooperative Adaptive Cruise Control (CACC) (Zhou et al., 2020), in which the CVs can concatenate with predecessors to form a string-stable cooperative vehicle platoon.

In the long-term, all vehicles will likely be equipped with V2V communications devices. It is expected to have a long transition period during which unequipped (non-communicating) and V2V-equipped vehicles would need to interact on the road, creating a mixed-flow traffic of human-driven vehicles (HDVs) and CVs. The development of CV-based safety and mobility applications should consider the effect of HDVs on performance in mixed-flow traffic. Specifically, platooning control of CVs in mixed-flow traffic can entail significant challenges, particularly arising from lane changes by HDVs. In a CV platoon, a CV may seek a sizeable transient spacing between itself and the preceding vehicle to improve safety and reduce speed fluctuations. However, a sizeable transient spacing can induce lane changes by HDVs in adjacent lanes, precluding the CV from achieving car-following equilibrium, and generating additional disturbances and oscillations in the traffic upstream. A real-world field test (Milanes et al., 2014) illustrates that during the platooning operation, the hardest deceleration occurs when an HDV lane change happens in front of the CV, as the reduced time headway due to the lane change creates a potential safety hazard that needs to be addressed quickly. This study labels such HDV lane changes that degrade the performance of the CV platooning control as "disruptive" lane changes. Lane changes are not only linked to capacity drop, traffic instability, and oscillations (Jin, 2010; Zheng et al., 2011), but also undermine traffic safety and induce crashes. Lane-change crashes account for 4 to 10 percent of all crashes (240,000 to 610,000 lane-change crashes per year), 0.5 to 1.5 percent of all motor-vehicle fatalities (224 to 732 fatalities per year), and almost 10 percent of all crash-caused delays (4.2 million hours) (Fitch et al., 2009). Hence, it is necessary to identify the presence of HDVs and their trajectories, understand lane-change interactions between CVs and HDVs, and analyze how CVs can leverage HDVs information to mitigate traffic oscillations and enhance safety in the CV platoon operations.

As the inherent heterogeneities and randomness in human behavior can generate disturbances in the traffic, previous studies spend numerous efforts to predict HDV lane changes to enhance safety. For

example, Wissing et al. (2017) propose a quantile regression-based approach to predict an upcoming lane change from adjacent vehicles on highways. Izquierdo et al. (2019) compared two lane change prediction models, one based on convolutional neural network (CNN) and the other based on long short-term memory (LSTM). Mahajan et al. (2020) develop an end-to-end learning-based framework to predict lane changes in real-time to enhance highway safety. While these studies may achieve the desired lane-change prediction accuracy, they do not control CVs to alleviate the adverse impacts of HDV lane changes. In this context, some studies develop longitudinal control models to address the consequences of the HDV lane changes passively; that is, they address the induced traffic oscillations after the lane change occurrence. Milanés and Shladover (2016) propose a time headway transition function in a cooperative adaptive cruise control system to handle HDV lane changes without causing significant perturbations. Bang and Ahn (2018) develop a spring mass damper system to mitigate the speed and spacing variation of the CV and its recovery time to reach the desired speed. Basiri et al. (2020) propose a distributed nonlinear model predictive control for CVs to handle the impact of HDV lane changes by maintaining desired spacings between vehicles. Zhao et al. (2020) use risk field theory to develop a human-like risk-response driver model for CVs to maintain road safety and traffic efficiency under lane changes. However, none of these studies proactively alleviate the adverse impacts before the HDV lane change occurs by leveraging CV longitudinal control. Jia et al. (2020) propose a car-following model for the CV to mimic the widely observed lane-change preclusion behavior of human drivers to proactively preclude HDV lane changes. However, it analyzes the influence of the HDV in an adjacent lane without factoring the HDV driving behavior prediction and real-time interactions between the CV and the HDV during the HDV lane-change process. In summary, the existing studies that passively handle the adverse outcomes of HDV lane changes do not consider the interactions between HDVs and CVs. Even the study that seeks to proactively preclude HDV lane changes does not leverage the HDV lane-change related traffic information (such as lane change intention) available to CVs to proactively preclude the occurrence of disruptive lane changes, which would enhance the smoothness of ambient traffic more effectively compared to the passive approaches.

In this context, this study proposes a deep reinforcement learning-based proactive longitudinal control strategy (PLCS) for CVs to proactively (i.e., before the execution of an HDV lane-change maneuver) reduce the occurrence of lane-change traffic conditions (in terms of spacing, speed difference, and accelerations) that will induce disruptive lane changes (i.e., cause abrupt braking by the CV and oscillations in the CV platoon) by adjacent HDVs.

In it, a Transformer-based lane-change traffic condition predictor (LTC-predictor) (Vaswani et al., 2017) is first constructed to predict the longitudinal driving trajectory of HDVs, and whether an HDV will likely perform a disruptive lane change under the ambient traffic conditions. Based on this prediction, the CV addresses one of two possible scenarios. In the scenario where no disruptive lane change is predicted, an extended intelligent driver model (EIDM)-based car-following control model is activated for the CV to perform smooth car-following behavior under cooperative CV platooning control. The

EIDM is car-following control model to regulate the trajectories of CVs in a platoon to achieve string stability whereby spacing perturbation would be dampened upstream in the CV platoon, and a long-wave string stability criterion is used to constrain the parameters of the EIDM to alleviate traffic oscillations. In the alternative scenario that disruptive lane-change traffic conditions are indicated by the LTC-predictor, the Markov decision process (MDP) (Bellman, 1957) is adopted to model the interactions between the CV and the HDV during the possible HDV lane change. Then, a rainbow deep Q-network (RDQN) (Hessel et al., 2018)-based lane-change preclusion model is applied for the CV to alter the lane-change traffic conditions to preclude the disruptive HDV lane change under the MDP framework. The MDP is a discrete-time stochastic control process for modeling decision-making in situations where outcomes are partly random (here, due to the traffic environment) and partly under the control of the decision-maker (here, the CV). The RDQN learns the optimal policy in an off-policy manner (Sutton & Barto, 2018) which evaluates and improves a policy different from that used to generate the training data (i.e., the learning is from data "off" the policy). As the off-policy method does not always execute the best longitudinal command suggested by the optimal policy for the CV, it reduces training efficiency and prevents the CV from learning from mistakes in the real-world implementation. The proposed PLCS addresses this issue by integrating the RDQN with the LTC-predictor in the training process to accelerate training convergence. It assists the CV in exploring dangerous behaviors (e.g., motions inducing collisions) in CV-HDV interactions by generating virtual collision data from the LTC-predictor rather than executing dangerous behaviors during the model training in the real world. To smoothen the control transition from the lane-change preclusion model to the car-following control model, a time headway transition function is developed to preclude abrupt accelerations and decelerations during the control transition. This function also prevents the control strategy from causing additional oscillations in lane-change preclusion failure cases. It is important to note that the fundamental mechanism of the PLCS is not to control the CV to directly block a lateral lane-change maneuver initiated by the HDV. Instead, its aim is to proactively reduce the occurrence of traffic conditions amenable to disruptive lane change before the HDV initiates a lane-change maneuver, so that potentially disruptive HDV lane changes can be precluded without unsafe CV-HDV interactions.

The effectiveness of the PLCS is validated through numerical experiments using NGSIM data. Results indicate that the PLCS can accurately predict the HDV vehicle states, and effectively leverage the predicted HDV information in precluding disruptive lane changes of HDVs, ensuring safety, and improving the smoothness of mixed-flow traffic. Sensitivity analysis demonstrates the generalizability of this control strategy for different lane-change scenarios, CV control setups, and HDV driver types.

2. METHODOLOGY

We consider the three-lane freeway scenario shown in Fig. 1 consisting of CVs, HDVs and a CV platoon, where a HDV potentially seeks to change lanes in front of the platoon's lead vehicle. The CV platoon is in Lane 2, with the ego vehicle A (a CV) as its lead vehicle. Vehicle B (an HDV) is the target vehicle that may perform a disruptive lane change that affects the CV platoon's string stability. The following assumptions are used to design the PLCS: (i) CVs can obtain the kinematic state information (position, speed, and acceleration) of neighboring vehicles through sensing, vehicle-to-vehicle (V2V) communications, and vehicle state-estimation algorithms; (ii) CVs can precisely track the planned CV trajectories generated by the control strategy by perfectly executing longitudinal commands; (iii) vehicle B is the only vehicle performing a lane change during this period, and (iv) the control frequency of the PLCS is set to 10Hz, i.e., each time step is 0.1 seconds in the control process.

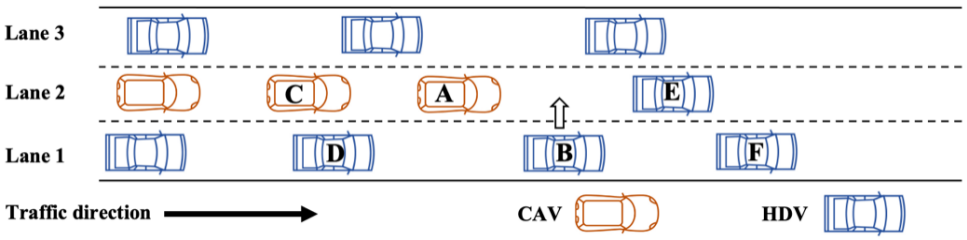

Figure 1. Problem illustration

2.1 PLCS framework

The PLCS follows the control logic illustrated in Fig. 2. First, the Transformer-based LTC-predictor predicts the future driving behavior of the target vehicle and the occurrence of traffic conditions for a potential disruptive lane change by it. If a "disruptive lane-change traffic condition" is predicted by the LTC-predictor, the RDQN-based lane-change preclusion model generates longitudinal commands for the ego vehicle to preclude such a disruptive lane change by the target vehicle. If "no disruptive lane-change traffic condition" is predicted, a control transition indicator is activated to determine whether a control transition from the lane-change preclusion model to the car-following control model has occurred for the ego vehicle. Such a control transition can undermine string stability of the CV platoon by inducing abrupt accelerations and decelerations in the ego vehicle. The indicator will indicate "no control transition" if the lane-change preclusion model has not been activated for the past few time steps (e.g., 10 seconds in the study experiments, based on Smith (1985)), as a prior control transition can require some time to be executed. Then, the EIDM-based car-following control model is used to control the ego vehicle to perform smooth car-following behavior. Otherwise, the indicator indicates a "control

transition"; then, the time headway transition function is used in conjunction with the car-following control model to smoothen the control transition from lane-change preclusion to car-following control by avoiding abrupt accelerations and decelerations.

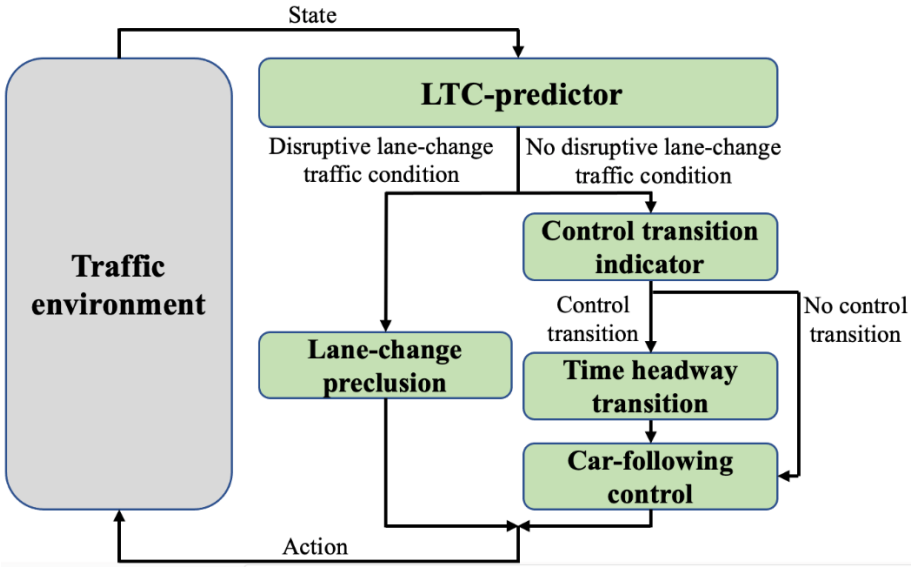

Figure 2. PLCS framework

2.2 Lane-change traffic condition predictor

The LTC-predictor predicts the future driving behavior of the target vehicle (e.g., acceleration), and then indicates whether the future traffic state in its vicinity (e.g., spacings, speeds, and accelerations of neighboring vehicles) can imply a disruptive lane-change traffic condition. The prediction of the driving behavior and lane-change traffic condition are implemented using a Transformer model (Vaswani et al., 2017). The Transformer model is a deep learning model based entirely on self-attention mechanisms, and differentially weighs the significance of each part of the input data. Compared to other recent learning models, it allows significantly more parallelization and achieves much higher training efficiency by processing sequential inputs (i.e., sequential traffic states in past time steps) as a whole and applying self-attention for information dependency. These characteristics enable the Transformer model to achieve high prediction accuracy for the target vehicle's driving behavior and disruptive lane-change traffic conditions.

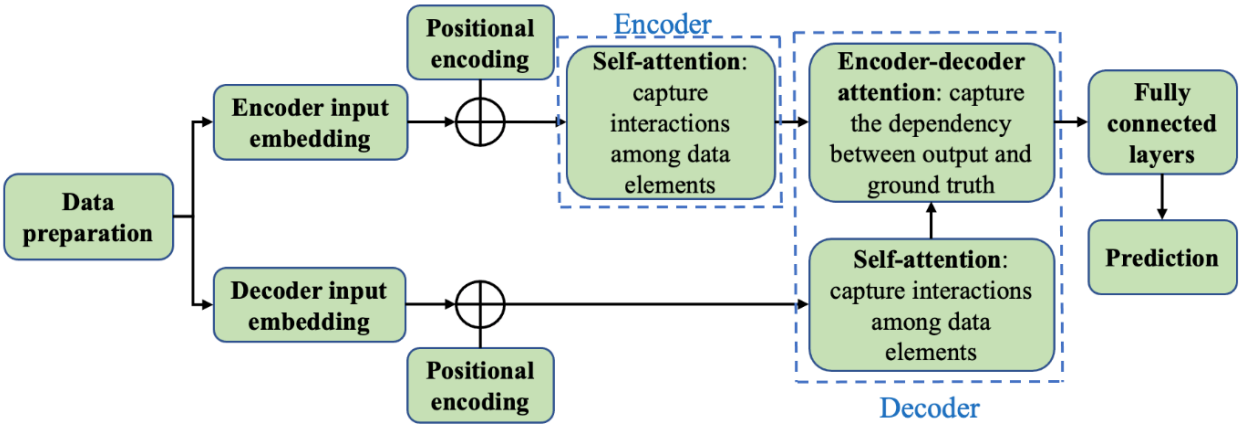

Figure 3. The LTC-predictor framework

The LTC-predictor use the traffic information in past few time steps to predict the driving behavior of the target vehicle and the disruptive lane-change traffic condition in the next time step. The framework of the Transformer-based LTC-predictor is illustrated in Fig. 3, and it works as follow. First, the traffic data is processed through the data preparation module, and shaped as input sequence, i.e., a sequence of input data at each time step (e.g., spacings, speeds, and accelerations of involved vehicles), and output sequence, i.e., a sequence of prediction results at each time step. This input sequence enters the encoder input embedding module as the input for the prediction process, and the output sequence enters the decoder input embedding module as the ground truth. Second, the embedding module reshapes the input sequence into sequences with a fixed dimension to fit the Transformer input structure, and the positional encoding module assigns positional information to all elements of the input sequence (i.e., the spacing, speed, and acceleration information). The positional information allows the Transformer to leverage the dependencies between the elements. Third, the encoder module activates attention mechanism via the self-attention layer to capture interactions among elements of the input sequence, by calculating their attention score. The attention score is defined as follows.

$$Attention(E, K, V) = softmax(\frac{EK^T}{\sqrt{d_k}})V \quad (1)$$

where, E, K, and V are the query, key, and value vectors of the input sequence, generated by multiplying the input sequence by query, key, and value weight matrices, which are randomly initialized. d_k is the dimension of the key vector. In practice, the key and value vectors represent the input sequence, and the query vector refers to a specific element in the input sequence. The dot product obtains the similarity between the specific element and the input sequence by probability vector, the softmax function normalizes the probability vector, and the multiplication of value vector generates a weighted

representation of the input sequence. The higher attention scores the elements obtain, the more important their interactions are in the prediction. Similarly, the self-attention layer in the decoder module is used to capture the interaction among elements of the ground-truth data. Fourth, the encoder-decoder attention layer in the decoder module activates the attention mechanism to capture the dependency between the predicted output and the ground-truth data. Finally, the fully connected layer module would process the output from the decoder module into the prediction of driving behaviors or disruptive lane-change traffic conditions. Please see the detailed descriptions of the Transformer modules in Vaswani et al. (2017).

Specifically, for the target vehicle's driving behavior prediction, the LTC-predictor uses the current speed of the target vehicle, and the speed difference and spacing between the target vehicle and the ego vehicle's preceding vehicle (vehicle E in Fig. 1) in previous time steps, to obtain the acceleration of the target vehicle in the next time step. For predicting a disruptive lane-change traffic condition, the LTC-predictor uses spacings between the target vehicle and its preceding vehicle (vehicle F in Fig. 1), the target vehicle and the ego vehicle, and the target vehicle and vehicle E, and speeds and accelerations of the target vehicle, ego vehicle, vehicle E, and vehicle F to indicate whether traffic conditions will induce a disruptive lane change by the target vehicle.

2.3 Car-following control model

When the traffic conditions do not imply potential disruptive lane changes by the target vehicle and the control transition indicator indicates "no control transition," the ego vehicle is controlled by the EIDM-based car-following control model. The goal of the car-following control model is to regulate the trajectories of CVs in a platoon to achieve string stability whereby spacing perturbation would be dampened upstream in the CV platoon. As shown in Fig. 4, in the implementation of the EIDM, the ego vehicle n (the CV with the rectangular box), which is vehicle A in Fig. 1, can receive position and speed information of the preceding HDV through onboard sensors, and obtain its acceleration information through vehicle state-estimation algorithms (assumption in Section 2.1).

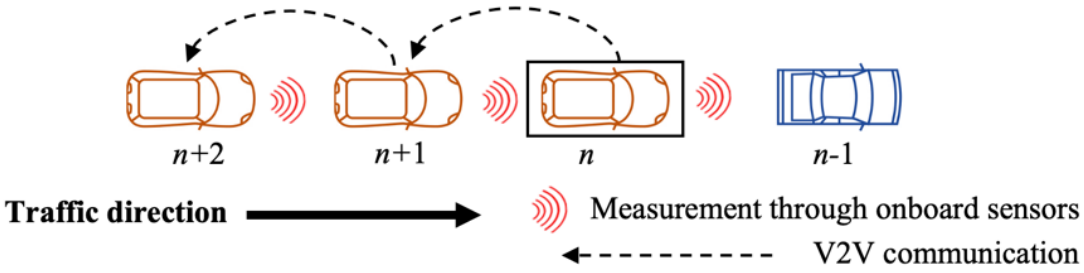

Figure 4. Implementation of EIDM

Other CVs, e.g., vehicle $n+1$, can receive position, speed, and acceleration information of their preceding CVs through onboard sensors and V2V communications.

Correspondingly, the dynamics of a CV under the EIDM-based car-following control model are as follows.

$$\dot{s}_n(t) = v_{n-1}(t) - v_n(t) \tag{2a}$$

$$\dot{v}_n(t) = F\left(v_n(t), s_n(t), \dot{s}_n(t), \ddot{s}_n(t)\right) \tag{2b}$$

where $F(v_n, s_n, \dot{s}_n, \ddot{s}_n) = \phi a_0 \left[1 - \left(\frac{v_n(t)}{v_{des}}\right)^{\sigma} - \left(\frac{s^*\left(\dot{s}_n(t), v_n(t)\right)}{s_n(t)}\right)^2\right] + \psi \ddot{s}_n$ is the EIDM-based car-following control law which regulates the acceleration of the ego vehicle n.

It should be noted that the time index in this section is denoted as t for continuous time, while k in the previous section is used to denote discrete time steps. $v_n(t)$ and $v_{n-1}(t)$ are the speed of vehicles n and $n-1$, respectively. $s_n(t) = x_{n-1}(t) - x_n(t)$, $\dot{s}_n(t)$, and $\ddot{s}_n(t)$ are the spacing, speed difference, and acceleration difference between vehicles $n-1$ and n, respectively. $x_n(t)$ is the position of vehicle n. Also, $s^*\left(\dot{s}_n(t), v_n(t)\right) = s_0 + v_n(t)T_{des} - \frac{v_n(t)\dot{s}_n(t)}{2\sqrt{a_0 b_0}}$ is the desired spacing during the car-following process, where a_0 and b_0 are the maximum acceleration and the desired deceleration, respectively. s_0 is the jam spacing, v_{des} is the desired speed, T_{des} is the desired safe time headway (minimum time headway to guarantee no collision between the ego vehicle and its preceding vehicle), and σ is the free acceleration exponent. $\phi \in \mathbb{R}^+$ is the sensitivity coefficient corresponding to car-following interactions and influences the acceleration variation of vehicle n with respect to spacing $s_n(t)$ and speed difference $\dot{s}_n(t)$. $\psi \in \mathbb{R}^+$ is the sensitivity coefficient with respect to the acceleration difference and modulates the acceleration of vehicle n to maintain the same pace with the preceding vehicle $n-1$. Then we introduce the definition of head-to-tail string stability.

Definition 1: (Head-to-tail string stability) A N-vehicle $\mathcal{N}$ is head-to-tail string stable if the following condition holds (Feng et al., 2019):

$$\left\|G_{1,N}(i\omega)\right\|_{H_\infty} = \left\|\frac{v_N(i\omega)}{v_1(i\omega)}\right\|_{H_\infty} \leq 1 \tag{3}$$

where i is the complex number indicator, ω is the angular frequency. The head-to-tail string stability indicates that the speed perturbation will not be amplified from the first vehicle to the last vehicle in a platoon. Correspondingly, the parameters in EIDM-based car-following control model are tuned based on the following Lemma 1 to ensure the head-to-tail string stability of the CV platoon. The time variable (t) is omitted hereafter for simplicity.

Lemma 1: A N-vehicle CV platoon $\mathcal{N}$ is head-to-tail string stable if the following condition holds:

$$\sum_{n=1}^{N}(g_{n,2}+f_n^3)<0 \tag{4a}$$

$$\sum_{n=1}^{N}(g_{n,1}+f_n^4)\prod_{m\neq n}f_m^2+\sum_{p\neq q,q>p}(g_{p,2}g_{q,2}+f_p^3f_q^3)\prod_{m\neq p,q}f_m^2>0 \tag{4b}$$

where $g_{n,1}=(1+f_n^4)$, $g_{n,2}=(f_n^3-f_{n-1}^1+f_n^1)$, $f_n^1=-\phi a_0\left[\frac{\sigma}{v_{des}}\left(\frac{v_{eq}}{v_{des}}\right)^{\sigma-1}+\frac{2(s_0+v_{eq}T_{des})T_{des}}{{s_{eq}}^2}\right]$, $f_n^2=\phi\frac{2a_0(s_0+v_{eq}T_{des})^2}{{s_{eq}}^3}$, $f_n^3=\phi\frac{2a_0(s_0+v_{eq}T_{des})v_{eq}}{{s_{eq}}^2\sqrt{a_0b_0}}$, $f_n^4=\psi$, $n\in\mathcal{N}$.

Proof: The head-to-tail string stability analysis quantifies the variations of spacing perturbation in a N-vehicle CV platoon $\mathcal{N}$ at the car-following equilibrium expressed as:

$$u_{eq}=(v_n^e,s_n^e,\dot{s}_n^e,\ddot{s}_n^e),n\in\mathcal{N} \tag{5}$$

where $v_n^e=v_0$ is the desired operating speed, s_n^e is the desired spacing, $\dot{s}_n^e=0$ is the desired speed difference, and $\ddot{s}_n^e$ is the desired acceleration difference. The spacing perturbation is expressed as: $y_n=\delta x_{n-1}-\delta x_n$, where δx_{n-1} and δx_n are the position deviations from their desired ones at the car-following equilibrium. With the impact of spacing perturbation y_n, the speed of vehicle n becomes $v_n=v_n^e+\delta v_n$, the spacing becomes $s_n=s_n^e+y_n$, the speed difference becomes $\dot{s}_n=\dot{s}_n^e+\dot{y}_n$, and the acceleration difference becomes $\ddot{s}_n=\ddot{s}_n^e+\ddot{y}_n$. Next, we discuss how to ensure that the spacing perturbation is not amplified in the CV platoon $\mathcal{N}$.

First, we express the variations of spacing perturbation around the equilibrium u_{eq} as:

$$\ddot{y}_n=F(v_{n-1},s_{n-1},\dot{s}_{n-1},\ddot{s}_{n-1})-F(v_n,s_n,\dot{s}_n,\ddot{s}_n) \tag{6}$$

Then, we linearize $\ddot{y}_n$ around the car-following equilibrium (5) through Taylor's first-order approximation:

$$\begin{aligned}\ddot{y}_n=&F(v_{n-1}^e,s_{n-1}^e,\dot{s}_{n-1}^e,\ddot{s}_{n-1}^e)-F(v_n^e,s_n^e,\dot{s}_n^e,\ddot{s}_n^e)+(f_{n-1}^1-f_n^1)\dot{y}_n+(f_{n-1}^2y_{n-1}-f_n^2y_n)+\\&(f_{n-1}^3\dot{y}_{n-1}-f_n^3\dot{y}_n)+(f_{n-1}^4\ddot{y}_{n-1}-f_n^4\ddot{y}_n)\end{aligned} \tag{7}$$

where $f_n^1=-\phi a_0\left[\frac{\sigma}{v_{des}}\left(\frac{v_{eq}}{v_{des}}\right)^{\sigma-1}+\frac{2(s_0+v_{eq}T_{des})T_{des}}{{s_{eq}}^2}\right]$, $f_n^2=\phi\frac{2a_0(s_0+v_{eq}T_{des})^2}{{s_{eq}}^3}$,

$f_n^3=\phi\frac{2a_0(s_0+v_{eq}T_{des})v_{eq}}{{s_{eq}}^2\sqrt{a_0b_0}}$, $f_n^4=\psi$.

Correspondingly, because $F(v_{n-1}^e, s_{n-1}^e, \dot{s}_{n-1}^e, \ddot{s}_{n-1}^e) = F(v_n^e, s_n^e, \dot{s}_n^e, \ddot{s}_n^e) = 0$ at the car-following equilibrium (5), the following equality is obtained:

$$(1 + f_n^4)\ddot{y}_n + (f_n^3 - f_{n-1}^1 + f_n^1)\dot{y}_n + f_n^2 y_n = f_{n-1}^4 \ddot{y}_{n-1} + f_{n-1}^3 \dot{y}_{n-1} + f_{n-1}^2 y_{n-1} \quad (8)$$

Applying the ring-road long-wave string stability method (Ward, 2009), we consider the following exponential ansatz to factorize the spacing perturbation of vehicle n:

$$y_n(t) = A_n e^{i\omega n + \lambda t} \quad (9)$$

where A_n is the magnitude of the perturbation, i is the complex number indicator, ω is the angular frequency, and λ is the characteristic root reflecting the decay/growth of the spacing perturbation in the platoon. $\lambda > 0$ indicates string instability whereby the spacing perturbation grows upstream in the platoon, while $\lambda < 0$ implies string stability whereby the spacing perturbation is dampened upstream in the platoon. $\lambda = 0$ is referred to as the marginal string stability whereby the spacing perturbation remains the same upstream in the platoon.

Substituting Equation (9) into Equation (8):

$$A_n\left[g_{n,1}\lambda^2 + g_{n,2}\lambda + f_n^2\right] = A_{n-1}e^{-i\omega}(f_{n-1}^4\lambda^2 + f_{n-1}^3\lambda + f_{n-1}^2) \quad (10)$$

where $g_{n,1} = (1 + f_n^4)$, $g_{n,2} = (f_n^3 - f_{n-1}^1 + f_n^1)$. Correspondingly, we can aggregate the spacing perturbations of a N-vehicle CV platoon as:

$$(M_1\lambda^2 + M_2\lambda + M_3)A = 0 \quad (11)$$

where $A = [A_1, A_2, \ldots, A_N]^\intercal$, and M_1, M_2, and M_3 are expressed as follows:

$$M_1 = \begin{bmatrix} g_{1,1} & 0 & \cdots & 0 & -e^{-i\omega}f_N^4 \\ -e^{-i\omega}f_1^4 & g_{2,1} & 0 & \cdots & 0 \\ 0 & -e^{-i\omega}f_2^4 & g_{3,1} & \cdots & 0 \\ 0 & 0 & -e^{-i\omega}f_3^4 & \ddots & \vdots \\ 0 & 0 & \cdots & -e^{-i\omega}f_{N-1}^4 & g_{N,1} \end{bmatrix},$$

$$M_2 = \begin{bmatrix} g_{1,2} & 0 & \cdots & 0 & -e^{-i\omega}f_N^3 \\ -e^{-i\omega}f_1^3 & g_{2,2} & 0 & \cdots & 0 \\ 0 & -e^{-i\omega}f_2^3 & g_{3,2} & \cdots & 0 \\ 0 & 0 & -e^{-i\omega}f_3^3 & \ddots & \vdots \\ 0 & 0 & \cdots & -e^{-i\omega}f_{N-1}^3 & g_{N,2} \end{bmatrix},$$

$$M_3 = \begin{bmatrix} f_1^2 & 0 & \cdots & 0 & -e^{-i\omega} f_N^2 \\ -e^{-i\omega} f_1^2 & f_2^2 & 0 & \cdots & 0 \\ 0 & -e^{-i\omega} f_2^2 & f_3^2 & \cdots & 0 \\ 0 & 0 & -e^{-i\omega} f_3^2 & \ddots & \vdots \\ 0 & 0 & \cdots & -e^{-i\omega} f_{N-1}^2 & f_N^2 \end{bmatrix}.$$

To ensure Equation (10) is valid**Error! Reference source not found.**, we require the determinant of $M_1\lambda^2 + M_2\lambda + M_3$ to be zero:

$$\det(M_1\lambda^2 + M_2\lambda + M_3) = \prod_{n=1}^{N}\left(g_{n,1}\lambda^2 + g_{n,2}\lambda + f_n^2\right) + e^{-iN\omega}\prod_{n=1}^{N}(f_n^4\lambda^2 + f_n^3\lambda + f_n^2) = 0 \quad (12)$$

To solve Equation (12), we expand the characteristic root λ and $e^{-iN\omega}$ into the power series solutions:

$$\lambda = i\lambda_1\omega + \lambda_2\omega^2 + \mathcal{O}(\omega^3) \quad (13a)$$

$$e^{-iN\omega} = 1 - iN\omega - \frac{N^2}{2}\omega^2 + \mathcal{O}(\omega^3) \quad (13b)$$

where $\mathcal{O}(\omega^3)$ represents the higher order terms which can be omitted.

Substituting Equations (13a) and (13b) into Equation (12), we have the following equality for the first-order characteristic root:

$$\mathcal{O}(\omega) = i\lambda_1\sum_{n=1}^{N} g_{n,2}\prod_{m\neq n} f_m^2 + i\lambda_1\sum_{n=1}^{N} f_n^3\prod_{m\neq n} f_m^2 - iN\prod_{n=1}^{N} f_n^2 \quad (14)$$

Thus, by setting $\mathcal{O}(\omega) = 0$, the first-order characteristic root is computed as:

$$\lambda_1 = \frac{N\prod_{n=1}^{N} f_n^2}{\sum_{n=1}^{N}(g_{n,2}+f_n^3)\prod_{m\neq n} f_m^2} \quad (15)$$

Similarly, for the second-order characteristic root, we have the following equality:

$$\mathcal{O}(\omega^2) = \sum_{n=1}^{N}\left(-g_{n,1}\lambda_1^2 + g_{n,2}\lambda_2\right)\prod_{m\neq n} f_m^2 - \lambda_1^2\sum_{p\neq q,q>p} g_{p,2}g_{q,2}\prod_{m\neq p,q} f_m^2 + \sum_{n=1}^{N}(-f_n^4\lambda_1^2 + f_n^3\lambda_2)\prod_{m\neq n} f_m^2 - \lambda_1^2\sum_{p\neq q,q>p} f_p^3 f_q^3\prod_{m\neq p,q} f_m^2 + N\lambda_1\sum_{n=1}^{N} f_n^3\prod_{m\neq n} f_m^2 - \frac{N^2}{2}\prod_{n=1}^{N} f_n^2 \quad (16)$$

By setting $\mathcal{O}(\omega^2) = 0$, the second-order characteristic root is determined as:

$$\lambda_2 = \frac{B\lambda_1^2 - \lambda_1 N\sum_{n=1}^{N} f_n^3\prod_{m\neq n} f_m^2 + \frac{N^2}{2}\prod_{n=1}^{N} f_n^2}{\sum_{n=1}^{N}(g_{n,2}+f_n^3)\prod_{m\neq n} f_m^2} \quad (17)$$

where $B = \sum_{n=1}^{N}(g_{n,1} + f_n^4)\prod_{m\neq n} f_m^2 + \sum_{p\neq q,q>p}(g_{p,2}g_{q,2} + f_p^3 f_q^3)\prod_{m\neq p,q} f_m^2$.

As the characteristic root needs to be negative for string stability, and $f_n^1 < 0$, $f_n^2 \geq 0$, $f_n^3 \geq 0$, $f_n^4 > 0$, then, to ensure $\lambda_1 < 0$, the following inequality needs to be satisfied:

$$\sum_{n=1}^{N}(g_{n,2} + f_n^3) < 0 \tag{18}$$

To guarantee $\lambda_2 < 0$, we further require $B\lambda_1^2 - \lambda_1 N \sum_{n=1}^{N} f_n^3 \prod_{m\neq n} f_m^2 + \frac{N^2}{2}\prod_{n=1}^{N} f_n^2 > 0$, which can be realized by the following inequality:

$$\sum_{n=1}^{N}(g_{n,1} + f_n^4)\prod_{m\neq n} f_m^2 + \sum_{p\neq q, q>p}(g_{p,2}g_{q,2} + f_p^3 f_q^3)\prod_{m\neq p,q} f_m^2 > 0 \tag{19}$$

Thereby, to ensure the head-to-tail string stability of a CV platoon, we require inequalities (18) and (19) to be valid. This completes the proof. ■

Note that the string stability region (4) can be applied to both homogeneous (i.e., vehicles in a platoon share the same parameters) and heterogenous CV platoons to tune the parameters of each CV in the platoon, which enables flexibility for real-world applications.

2.4 Lane-change preclusion model

If the traffic environment is identified as satisfying the traffic condition for a disruptive lane change by the target vehicle, the lane-change preclusion model takes over and controls the ego vehicle to preclude the potential HDV lane change. To develop the lane-change preclusion model, first, the interactions between the CV and the HDV in the traffic environment are modeled using the Markov decision process (MDP) (Bellman, 1957). As shown in Fig. 5, the goal of an MDP is to obtain the optimal policy that specifies actions to maximize a reward function.

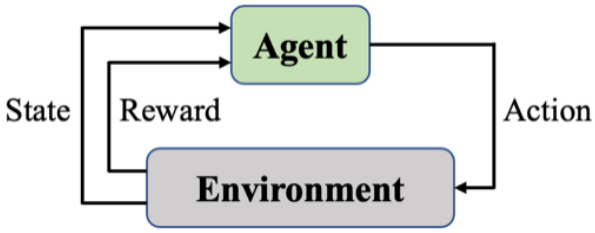

Figure 5. MDP framework

Here, the agent is the ego vehicle, and the environment is the traffic environment around the ego vehicle, i.e., the scenario including the ego vehicle, the target vehicle, and the neighboring vehicles C, D, E, and F as shown in Fig. 1. The "state" refers to the positions and speeds of vehicles in the traffic environment, denoted as $\boldsymbol{z} = [\boldsymbol{z}^C, \boldsymbol{z}^E, \boldsymbol{z}^{ego}, \boldsymbol{z}^{tar}, \boldsymbol{z}^F, \boldsymbol{z}^D]$, where $\{\boldsymbol{z}^i = [x_i, v_i] | i = C, E, ego, tar, F, D\}$ represent vehicle states, their superscripts/subscripts C, E, ego, tar, F, and D refer to vehicle C, vehicle E, the ego vehicle, the target vehicle, vehicle F, and vehicle D shown in Fig. 1, and x_i, v_i are positions and speeds of the corresponding vehicles. The "action", denoted as u, is specified as the controlled acceleration a of the ego vehicle. In this study, we define the action u in a discrete action space U, i.e., $u \in U$, of which the specific values will be discussed later in the numerical experiments section. The reward function is designed to: (i) preserve traffic smoothness in the CV platoon by precluding potential disruptive lane changes by the target vehicle, (ii) ensure safety of the ego vehicle, (iii) ensure motion comfort of the ego vehicle, and (iv) ensure the speed homogeneity of the CV platoon. The reward function at each time step k is defined as follows.

$$R(k) = R_l(k) + R_c(k) + R_s(k) + R_a(k) + R_v(k) \tag{20}$$

The components of the reward function are:

(1) Cost of a disruptive lane change by the target vehicle: $R_l(k) = \theta_l \cdot LC(k)$, where $LC(k) = \{0,1\}$ (0 indicates the occurrence of a disruptive lane change by the target vehicle at current time step k, and 1 otherwise). θ_l is a positive scaling parameter to ensure that the lane-change reward component is of comparable magnitude to other reward components in Equation (20). Similar scaling parameters $\{\theta_j | \theta_j > 0, j = l, s, a, v\}$ are specified for most of the other reward components as well. The scaling parameters are determined based on a trial-and-error method to achieve the desired lane-change preclusion performance while retaining smoothness and safety. Their specific values will be discussed later in the numerical experiments section. Reward component $R_l(k)$ fosters the preclusion of a disruptive lane change by the target vehicle so that traffic smoothness can be preserved for the CV platoon.

(2) Cost of safety of the ego vehicle: $R_c(k) = \begin{cases} -\delta, & s(k) < s_{\text{safe}} \; or \; v(k) < 0 \\ 0, & \text{otherwise} \end{cases}$, where $s(k)$ is the spacing between the ego vehicle and its preceding vehicle at current time step k, s_{safe} is the minimum spacing to guarantee no collision between the ego vehicle and its preceding vehicle , and $v(k)$ is the current speed of the ego vehicle. δ ($\delta > 0$) is a large enough penalty value to ensure that undesired situations ($s(k) < s_{\text{safe}} \; or \; v(k) < 0$) will not occur.

(3) Cost of spacing between the ego vehicle and its preceding vehicle: $R_s(k) = \begin{cases} \theta_s \cdot \left(\frac{s(k)}{s_{\text{des}}}\right)^2, \text{ if } s(k) \leq s_{\text{des}} \\ \theta_s \cdot \left(\frac{s_{\text{des}}}{s(k)}\right)^2, \text{ otherwise} \end{cases}$, where s_{des} is the desired spacing between the ego vehicle and its preceding vehicle. This reward component complements the lane-change preclusion and safety reward components by maintaining the desired spacing to avoid lane changes by the target vehicle due to large spacings or crashes due to small spacings.

(4) Cost of motion comfort of the ego vehicle: $R_a(k) = \theta_a \cdot \left(1 - \frac{|a(k) - \bar{a}(k)|}{a_{\max} - a_{\min}}\right)^2$, where $a(k)$ is the acceleration of the ego vehicle at current time step k, $\bar{a}(k)$ is the average longitudinal acceleration of the ego vehicle in the past few time steps (e.g., 5 seconds), and $a_{\max}$ and $a_{\min}$ are the maximum and minimum accelerations that the ego vehicle can apply, respectively. This reward component ensures motion comfort of the ego vehicle.

(5) Cost of speed homogeneity: $R_v(k) = \begin{cases} \theta_v \cdot \left(1 - \frac{|v(k) - v_{\text{pre}}(k)|}{v_{\text{pre}}(k)}\right)^4, \text{if } |v(k) - v_{\text{pre}}(k)| \leq v_{\text{pre}}(k) \\ 0, \text{ otherwise} \end{cases}$, where $v_{\text{pre}}(k)$ is the target speed of the ego vehicle (i.e., the mean speed of the preceding vehicle in the immediate past time step). This reward component ensures the speed homogeneity of the CV platoon.

It is challenging to solve the MDP problem in the context of mixed-flow traffic, as the future driving behaviors of HDVs are unknown to the ego vehicle. To handle such an unknown environment, we use a reinforcement learning (RL) framework (Sutton & Barto, 2018) to solve the MDP problem. RL is a strong artificial intelligence (AI) paradigm which teaches the ego vehicle based on interactions with the traffic environment and learning from mistakes. A commonly used value-based RL algorithm, Q-learning (Watkins & Dayan, 1992) is adopted in this study, as Q-learning enables learning from past memory (i.e., historical traffic data). The Q-learning algorithm introduces a Q-function to map the state-action pair and Q-value to generate the optimal policy; here, Q-value is defined as the expected cumulative reward from taking a certain action in the current state and acting optimally thereafter. The Q-value at time step k can be expressed as:

$$Q(\boldsymbol{z}(k), u(k)) = R(k) + \gamma \cdot \max_{u(k+1)} Q(\boldsymbol{z}(k+1), u(k+1)) \quad (21)$$

where $\boldsymbol{z}(k)$ and $u(k)$ are the state and action at the current time step k in the lane-change process, respectively, and γ is the discount factor which determines how important future rewards are to the current state.

The Q-learning algorithm updates the Q-function based on the Bellman equation (Bellman, 1957),

$$Q(\boldsymbol{z}(k), u(k)) \leftarrow (1-\eta) \cdot Q(\boldsymbol{z}(k), u(k)) + \eta \cdot [R(k) + \gamma \cdot \max_{u(k+1)} Q(\boldsymbol{z}(k+1), u(k+1))] \quad (22)$$

where η is the learning rate, i.e., the step size of the ego vehicles' Q-function update during model training. The Q-function is updated iteratively until convergence.

The Q-learning-based algorithm used here is the state-of-the-art rainbow deep Q-network (RDQN) algorithm (Hessel et al., 2018). The RDQN combines the latest improvements in deep Q-network algorithms, e.g., double Q-learning, dueling networks, multi-step bootstrapping, prioritized replay buffer, distributional RL, noisy deep Q-network, etc., gaining high performance in Q-value estimation, learning efficiency, bias-variance trade-off, and control policy exploration (Hessel et al., 2018). In this study, we incorporate the RDQN with the convolutional neural network (CNN) (Mnih et al., 2013, Schmidhuber, 2015) to deal with the numerous states and actions in this MDP problem and capture the structural information in the state $\boldsymbol{z}$, which is two-dimensional array consisting of position and speed information of all involved vehicles following a specific order to represent connections among vehicles.

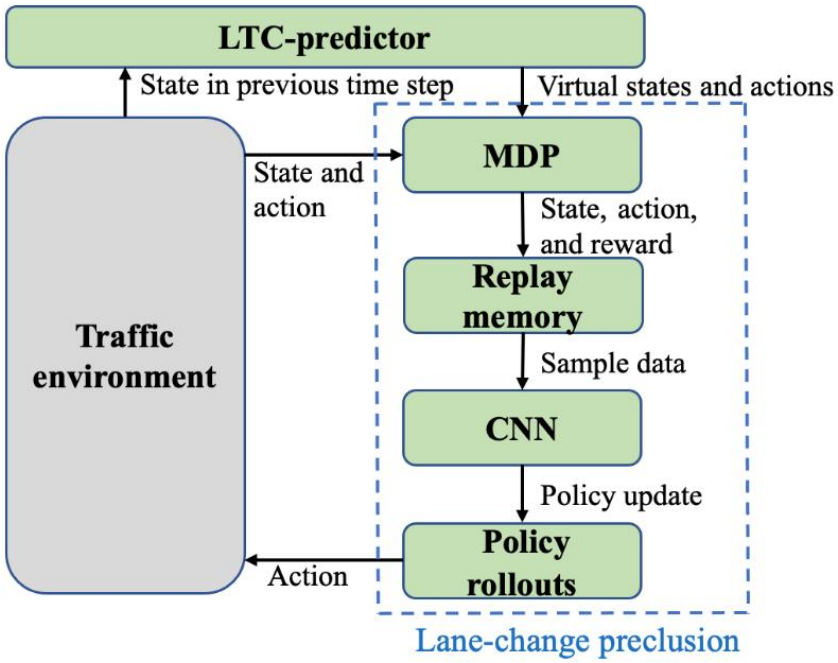

Figure 6. Integration of LTC-predictor with RDQN model training

The RDQN obtains only one training sample of a specific action executed by the ego vehicle at each time step in the model training process, limiting sampling productivity and training efficiency. Moreover, the training process of Q-learning-based algorithms is relatively expensive, specially, in the beginning steps, as state-action pairs need to be visited frequently to converge to the optimal policy (Pouyan et al., 2014). Thus, a large amount of training samples over the whole action space at each time step can significantly improve training efficiency of the RDQN. To this end, the PLCS integrates the RDQN with the LTC-predictor in the training process to accelerate training convergence, as shown in Fig. 6. The RDQN-based lane-change preclusion model consists of four modules: a MDP module that generates rewards corresponding to given states and actions, a replay memory module storing state-action-reward data (i.e., training data) for model training, a CNN module (i.e., deep neural network) (Schmidhuber, 2015) updating the new control policy for the ego vehicle, and a policy rollouts module (i.e., action generator) generating new actions of the ego vehicle in the traffic environment. Specifically, an epsilon greedy algorithm is applied in the policy rollouts module to balance the exploitation of actions generated by the trained control policy and exploration of any available actions in the action space. The epsilon ϵ refers to the probability of choosing exploration, that is, the algorithm performs exploration with probability ϵ and exploitation with probability $1-\epsilon$. The ϵ is set with a large value for more explorations in the beginning stage of the training process and then decay to a small value for more exploitations. In the conventional model training process of the RDQN, after the action execution by the ego vehicle in previous time step, the ego vehicle detects the current state $\boldsymbol{z}$ newly generated by the traffic environment and sends it to the MDP module. The MDP module generates the corresponding reward R for the received state $\boldsymbol{z}$ and executed action u, and passes the state-action-reward data, i.e., a training sample $\boldsymbol{d} = [\boldsymbol{z}, u, R]$, to the replay memory module. Then, the replay memory module feeds the CNN module with training samples, and a new control policy for the ego vehicle is generated by the CNN module and updated to the policy rollouts module for a new action generation. The newly generated action is then executed by the ego vehicle in the traffic environment. This iterative procedure is repeated until the convergence of the CNN module is reached.

However, the conventional RDQN training collects only one training sample for the executed action of the ego vehicle at each time step, limiting training efficiency. In our study, the integrated LTC-predictor generates additional training samples to accelerate the training convergence, as shown in Fig. 6. Based on the state in the previous time step, the LTC-predictor predicts virtual states over all possible actions (instead of only one action executed by the ego vehicle), sends them to the MDP module for reward generations, and passes the virtual training samples $\{\tilde{\boldsymbol{d}}\}$ over all possible actions to the replay memory module, where $\tilde{\boldsymbol{d}} = [\tilde{\boldsymbol{z}}, \tilde{u}, \tilde{R}]$ represent a virtual training sample for any possible action $\tilde{u} \in U$, the corresponding virtual state $\tilde{\boldsymbol{z}}$, and reward $\tilde{R}$. Hence, the replay memory module collects not only one training sample $\boldsymbol{d}$ from the executed action by the ego vehicle, but also virtual training samples $\{\tilde{\boldsymbol{d}}\}$ over all possible actions without actual executions, enhancing the training data exploration of the RDQN and accelerating the training convergence.

Remark 1: To maintain safety during real-world implementation, the conventional RDQN prevents the ego vehicle from executing dangerous behaviors (e.g., actions inducing collisions) in the CV-HDV interactions, and sequentially suppresses learning from mistakes adaptively with real-time collision data. This can significantly undermine the safety performance of the RDQN in the real world. By contrast, in the PLCS, the integrated LTC-predictor generates virtual training data induced from dangerous behaviors. This enables the ego vehicle to learn from mistakes adaptively while circumventing the execution of dangerous behaviors in CV-HDV interactions, which further enhances the safety performance of the RDQN in different traffic conditions.

2.5 Time headway transition function

If the LTC-predictor does not predict potential disruptive lane changes by the target vehicle and the control transition indicator indicates "control transition", the time headway transition function is activated to assist the car-following control model to smoothen the control transition from lane-change preclusion to car-following control. As the ego vehicle needs to accelerate to reduce the spacing to achieve lane-change preclusion, this induces a large speed for the ego vehicle and a small spacing between it and its preceding vehicle. This phenomenon further leads to the ego vehicle's abrupt deceleration when it switches from the lane-change preclusion model to the car-following control model. Remarkably, if lane-change preclusion control fails to preclude a disruptive lane change by the target vehicle, the ego vehicle will switch back to car-following control to deal with the lane change by the target vehicle. This will cause abrupt decelerations by the ego vehicle as the lane-change preclusion model further reduces the spacing during the control process, which leads to even smaller time headways after failing to preclude the lane change by the target vehicle.

To mitigate the potential oscillations generated by the non-smooth control transition from the lane-change preclusion model to the car-following control model, this study proposes a time headway transition function to adjust the desired time headway of the car-following control model. This function is inspired by the lane-change relaxation phenomenon of human drivers (Smith, 1985), where a human driver would initially accept a smaller time headway when experiencing a cut-in, then gradually recover to the original desired time headway (this process typically lasts for 20-30 seconds). The time headway transition function is specified as follows:

$$T(t) = \max\{T_0, T_{min}\} + \frac{t}{H}(T_{des} - \max\{T_0, T_{min}\}), \tag{23}$$

where T_0 is the zero-acceleration time headway at the start of the control transition. T_0 stimulates the car-following control model to generate an action of zero acceleration (i.e., Equation (2b) equals zero) given the current speed. T_{min} denotes the minimum time headway to guarantee the safety of the ego vehicle. Its value depends on the operating speed and vehicle braking capability in real-world implementation (e.g., the time for the ego vehicle to decelerate to the speed of its preceding vehicle

using the maximum braking power). T_{des} denotes the original desired time headway of the ego vehicle. $T(t)$ is the new desired time headway at time t, and H refers to the dwelling time length of the control transition. Equation (23) states that after the lane-change preclusion is completed, the ego vehicle first applies the car-following control model with the time headway T_0 to preclude an undesired abrupt deceleration (proved by lemma 2). Then, it linearly adjusts the desired time headway to approach the original desired time headway T_{des} after a dwelling time of H, without jeopardizing the local stability1 and string stability of the car-following control model (proved by lemmas 2 and 3). Note that increasing H can potentially reduce speed fluctuations during the control transition, but it can take longer to recover to the original desired time headway. Hence, a large H is undesirable as it makes the car-following control model work under a smaller time headway for longer time, which can jeopardize string stability performance in the car-following control process.

As the car-following control model is implemented based on the EIDM, the zero-acceleration time headway T_0 is correspondingly derived as:

$$T_0 = \frac{s_n}{v_n}\sqrt{1-\left(\frac{v_n}{v_{des}}\right)^{\sigma}+\frac{k_g\ddot{s}_n}{a_0}}-\frac{s_0}{v_n}+\frac{\dot{s}_n}{2\sqrt{a_0 b_0}}. \tag{24}$$

Lemma 2: The time headway transition function can ensure smaller deceleration during the control transition.

Proof: After the execution of lane-change preclusion, the spacing between the ego vehicle and its preceding vehicle shrinks to a value $s_n^{preclusion}$. Because $s_n^{preclusion}$ is smaller than the equilibrium spacing s_n^e, the EIDM-based car-following control model will cause a large deceleration $a_{brake}^{preclusion}$:

$$a_{brake}^{preclusion} = \phi a_0\left[1-\left(\frac{v_n(t)}{v_{des}}\right)^{\sigma}-\left(\frac{s_0+v_n(t)T_{des}-\frac{v_n(t)\dot{s}_n(t)}{2\sqrt{a_0 b_0}}}{s_n^{preclusion}(t)}\right)^2\right]+\psi\ddot{s}_n \tag{25}$$

With the time headway transition function, the desired time headway is adjusted from T_{des} to $T(t) = \max\{T_0, T_{min}\} + \frac{t}{H}(T_{des} - \max\{T_0, T_{min}\})$. Correspondingly, the deceleration $a_{brake}^{transition}$ under the time headway transition function can be expressed as:

$$a_{brake}^{transition} = \phi a_0\left[1-\left(\frac{v_n(t)}{v_{des}}\right)^{\sigma}-\left(\frac{s_0+v_n(t)T_0-\frac{v_n(t)\dot{s}_n(t)}{2\sqrt{a_0 b_0}}}{s_n^{preclusion}(t)}\right)^2\right]+\psi\ddot{s}_n \tag{26}$$

[1] The local stability indicates that the spacing perturbation will decay to zero with time, instead of growing to unbounded values or fluctuating throughout the control process.

As $T_0 < T_{des}$, the spacing interaction term $s_0 + v_n(t)T_0 - \frac{v_n(t)\dot{s}_n(t)}{2\sqrt{a_0 b_0}}$ will be closer to $s_n^{preclusion}(t)$ than $s_0 + v_n(t)T_{des} - \frac{v_n(t)\dot{s}_n(t)}{2\sqrt{a_0 b_0}}$, which sequentially indicates that $\left|a_{brake}^{transition}\right| < \left|a_{brake}^{preclusion}\right|$. This completes the proof. ■

Lemma 3: The time headway transition function will not jeopardize the local stability of the EIDM-based car-following control model.

Proof: Akin to the proof of lemma 1, and assuming a homogeneous platoon, the variations of spacing perturbation around the car-following equilibrium can be expressed as:

$$\ddot{y}_n = f_n^1 \dot{y}_n + f_n^2 (y_{n-1} - y_n) + f_n^3 (\dot{y}_{n-1} - \dot{y}_n) + f_n^4 (\ddot{y}_{n-1} - \ddot{y}_n) \tag{27}$$

where $f_n^1 = -\phi a_0 \left[\frac{\sigma}{v_{des}}\left(\frac{v_{eq}}{v_{des}}\right)^{\sigma-1} + \frac{2(s_0 + v_{eq}T_{des})T_{des}}{{s_{eq}}^2}\right]$, $f_n^2 = \phi \frac{2a_0(s_0 + v_{eq}T_{des})^2}{{s_{eq}}^3}$, $f_n^3 = \phi \frac{2a_0(s_0 + v_{eq}T_{des})v_{eq}}{{s_{eq}}^2\sqrt{a_0 b_0}}$, $f_n^4 = \psi$. Correspondingly, in the Laplace domain, the transfer function from y_{n-1} to y_n can be expressed as:

$$\Gamma_{n-1,n}(\mathcal{s}) = \frac{Y_n(\mathcal{s})}{Y_{n-j}(\mathcal{s})} = \frac{f_n^4 s^2 + f_n^3 s + f_n^2}{(1 + f_n^4)s^2 + (f_n^3 - f_n^1)s + f_n^2} \tag{28}$$

where $\mathcal{s} = i\omega$ is the Laplace operator, i is the indicator of complex number, and ω is the angular frequency.

As $T(t) \geq T_0$, the time headway transition function (23) will not induce the desired time headway to be negative. Correspondingly, the following inequalities remain valid: $f_n^1 < 0$, $f_n^2 > 0$, $f_n^3 > 0$, $\psi > 0$. Thus, the characteristic roots of (28) are in the left-hand side of the imaginary axis, which ensures the local stability of the EIDM-based car-following control model. This completes the proof. ■

Remark 2: The proposed time headway transition function can smoothen the control transition from the lane-change preclusion model to the car-following control model. Further, it can also deal with disruptive cut-out and cut-in scenarios. Specifically, when the preceding vehicle suddenly leaves the existing platoon (i.e., changes lanes), or a vehicle abruptly cuts in front of the ego vehicle, the time headway transition function can assist the ego vehicle in dealing with the suddenly enlarged/reduced time headway in a smoother manner (i.e., mitigate the abrupt acceleration/deceleration).

3. NUMERICAL EXPERIMENTS

This section discusses numerical experiments to illustrate the performance of the PLCS and conduct sensitivity analyses. They are conducted using Python in a computational environment consisting of CPU core i9, 32GB RAM, and a RTX2080 GPU. A baseline strategy, defined as scenarios without lane-change preclusion (i.e., the ego vehicle is controlled only by the EIDM-based car-following control model), is used for comparison. To examine the generalizability of the PLCS, two different scenarios are considered, which generate large spacings and thus could induce lane changes: (i) a three-lane freeway scenario with vehicle E speeding, denoted as scenario 1 and shown in Fig. 7(a), and (ii) a three-lane freeway scenario with vehicle G cutting out, denoted as scenario 2 and shown in Fig. 7(b). Further, various CV control setups and HDV driver types are considered, as discussed hereafter.

3.1 Experiment setup

The two lane-change scenarios shown in Fig. 7 are used to conduct numerical experiments. Two 150-second trajectories and two 32-second trajectories in congested traffic (containing multiple stop-and-go movements) on I-80 freeway from the NGSIM dataset (Alexiadis et al., 2004), with a 10 Hz sampling frequency, are extracted as driving behaviors of vehicles E and F. Vehicle E in lane 2 has a higher average speed than vehicle F in lane 1, which would induce potential disruptive lane changes by vehicle B (the target vehicle) from lane 1 to lane 2.

The two 150-second trajectories (shown in Fig. 8) are designed for scenario 1 where the sizable spacing between the ego vehicle A and vehicle E is caused by the speeding of vehicle E (Fig. 7(a)) and induces the HDV lane change. The two 32-second trajectories (shown in Fig. 9) are designed for scenario 2 where the sizable spacing between the ego vehicle and vehicle E is caused by the cut-out behavior of vehicle G (Fig. 7(b)).

The initial speeds for the other vehicles are identical to those of their own preceding vehicles, initial accelerations are 0, and initial relative spacings of vehicles are set as:

$$s_j = (s_0 + v_j T)/\sqrt{1-(v_j/v_{des})^4},$$

where the desired speed v_{des} is 30 m/s, and j refers to vehicles A, B, C, and D.

In scenario 2, the experiment starts at the time when vehicle G cuts out, and there is sizable spacing between the ego vehicle and vehicle E that induces a potential lane change by vehicle B.

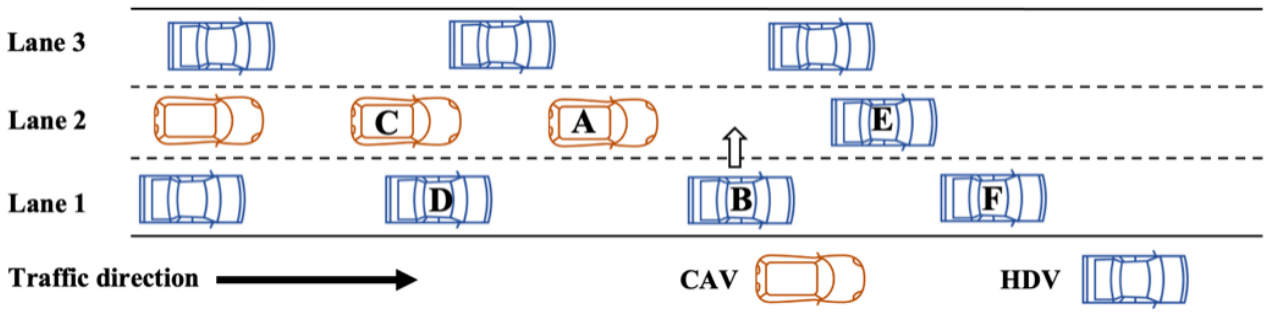

(*a*)

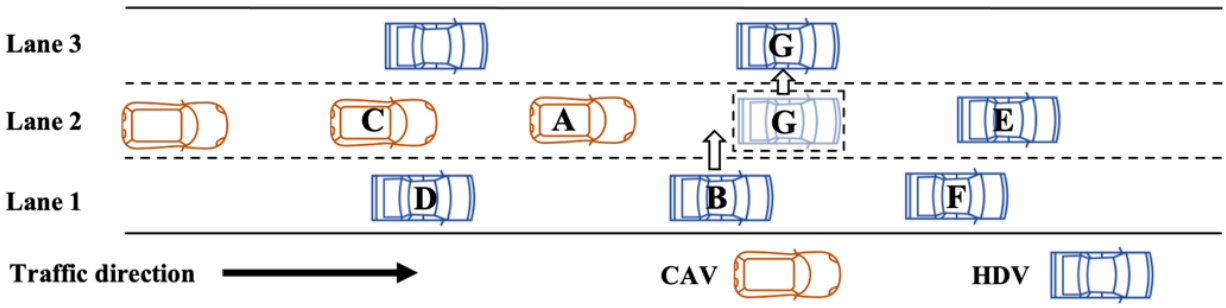

(*b*)

Figure 7. Lane-change scenarios: (a) scenario 1, and (b) scenario 2.

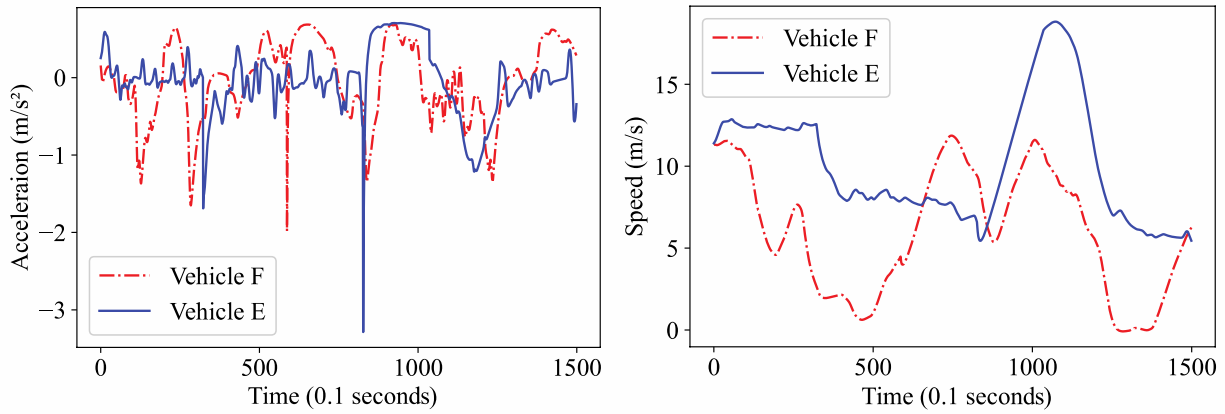

(*a*) (*b*)

Figure 8. Trajectories of vehicles E and F in scenario 1: (a) acceleration profile, and (b) speed profile

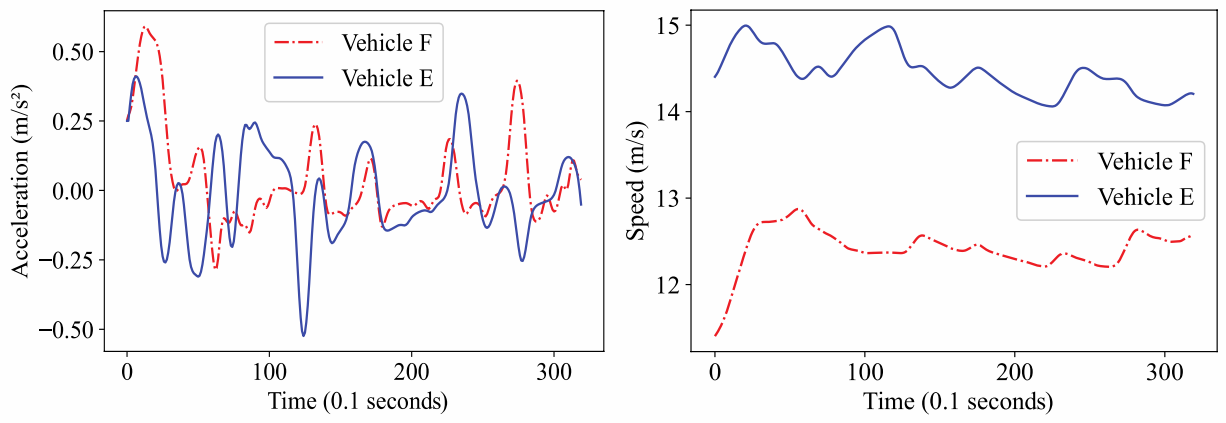

(*a*) (*b*)

Figure 9. Trajectories of vehicles E and F in scenario 2: (a) acceleration profile, and (b) speed profile

The following models are used to generate the vehicle dynamics for the experiments. For HDVs (except vehicles E and F), the IDM (Treiber et al., 2000) is used to simulate the car-following behaviors with parameters of three HDV driver types (cautious, normal, and aggressive drivers) from Zhu et al. (2019), as shown in Table 1. The lane-change decision-making of vehicle B is described by the MOBIL model (Kesting et al., 2007) with parameters specified in Table 2. The MOBIL is a heuristic function that suggests vehicle B to change lanes if an acceleration improvement after a lane change is greater than a threshold value (i.e., a lane-change traffic condition is satisfied). The lane-change trajectory planning of vehicle B is performed using a k-nearest-neighbors (KNN) model (Altman, 1992) with 370 lane-change trajectory samples extracted from the NGSIM dataset. For CVs, longitudinal commands are generated using the EIDM-based car-following control model of the PLCS.

Three parameter sets of the EIDM are sampled from the string stability region in Equation (7) to simulate three CV control setups, as shown in Table 3. EIDM1 refers to platooning control with relatively smaller spacings to achieve high traffic capacity but relatively lower speed dampening. EIDM3 represents platooning control with relatively larger spacings to gain more speed dampening but relatively lower traffic capacity, and EIDM2 is in between EIDM1 and EIDM3 (i.e., medium levels of spacing and speed dampening).

The experiments assume that vehicle B performs a lane change only if a lane-change time window (representing the persisting time steps of continuous lane-change suggestions from MOBIL) persists for at least 15 time steps (i.e., 1.5s, based on Finnegan & Green (1990)) and no potential collision occurs.

Table 1. Parameters of IDM

	T (s)	a_0 (m/s^2)	b_0 (m/s^2)	s_0 (m)
Aggressive	$\mathbb{N}(1.6, 0.2)$	$\mathbb{N}(1.05, 0.08)$	$\mathbb{N}(1.54, 0.08)$	$\mathbb{N}(2, 0.5)$
Normal	$\mathbb{N}(2.57, 0.2)$	$\mathbb{N}(0.87, 0.08)$	$\mathbb{N}(1.14, 0.08)$	$\mathbb{N}(2, 0.5)$
Cautious	$\mathbb{N}(3.16, 0.2)$	$\mathbb{N}(0.8, 0.08)$	$\mathbb{N}(1.08, 0.08)$	$\mathbb{N}(2, 0.5)$

where: $\mathbb{N}$ - normal distribution.

Table 2. Parameters of MOBIL

	p	b_{safe} (m/s^2)	Δa_{th} (m/s^2)
Aggressive	0	-8.0	0
Normal	0.05	-5.0	0
Cautious	0.05	-2.0	0

where: p – politeness factor,
b_safe – maximum safe deceleration,
Δa_{th} - lane-change threshold.

Table 3. Parameters of EIDM

	T (s)	a_0 (m/s^2)	b_0 (m/s^2)	s_0 (m)	ϕ	ψ
EIDM1	1.2	0.8	1.8	2	1	0.7
EIDM2	1.2	0.8	1.5	2	0.85	0.6
EIDM3	1.6	0.73	1.75	2	0.5	0.5

3.2 Model training

3.2.1 LTC-predictor

In this study, the LTC-predictor is constructed by concatenating a two-layer Transformer of width 256 with four attention heads, and three fully connected layers. The hidden size of the feed-forward network in the Transformer is set to 512, and the hidden sizes in fully connected layers are 256, 128, and 64, respectively. The dropout value of inputs is set to 0.1 and the sequence length is set to 5 time steps. We choose the mean-squared-error loss function for the prediction of the driving behavior, and the cross-entropy loss function for the disruptive lane-change traffic condition. The descriptions of the Transformer parameters are provided in Vaswani et al. (2017).

For LTC-predictor training, an experiment is conducted with an EIDM-driven CV (the ego vehicle) to generate 297,600 data points with disruptive lane changes as the ground truth, where the disruptive lane changes induce harsh braking and large speed fluctuations to the following vehicle. Specifically, the generated traffic conditions (in terms of spacing, speed difference, and accelerations), which obtain lane-change suggestions from MOBIL and later induce disruptive lane changes, are used as the disruptive lane-change traffic conditions for the LTC-predictor training. The detailed description of the input and output data of the LTC-predictor has been introduced in Section 3.1. In the experiments, 80% of the generated data are used for training, 10% for validation, and the remaining 10% for testing.

3.2.2 Lane-change preclusion model

The neural network architecture of the RDQN in the lane-change preclusion model, as shown in Fig. 10, is constructed by concatenating three CNN layers (hidden states of 32, 64, 128) with dropout value of 0.2 and three fully connected layers (hidden states of 896, 512, 512) with dropout value of 0.5. As the dimension of input in the RDQN is not very high, we do not consider pooling layers in the CNN layers. The architecture works as follow. First, the input data (state $\boldsymbol{z}$ in the MDP) enters the CNN layers and experiences three convolutions: the first convolution with kernel size of 3, stride of 1, and padding of 1; the second convolution with kernel size of 2, stride of 1, and padding of 0; and the third convolution with kernel size of 2, stride of 1, and padding of 0. Then, the output from the CNN layers will be shaped into vectors and processed by the fully connected layers. Finally, the fully connected layers generate the output as Q values over the action space, and the action with the maximum Q value would be selected by the ego vehicle for action execution.

In this study, the action u of the lane-change preclusion model is defined in a discrete space U from -2.00 to 2.00 with a common difference of 0.01, i.e., $U = \{-2.00, -1.99, \ldots, 1.99, 2.00\}$. The other hyperparameters of the lane-change preclusion model are tuned for optimal training convergence, as shown in Table 4. The learning rate is set to 0.0001, the total number of training episodes is 1000, the discount factor is 0.95, the batch size for training is 5120, and we update the neural network in the

RDQN every 10 episodes. During the model training, to balance the trade-off between the early exploration and later exploitation of the RDQN control policy, the ϵ in the epsilon greed algorithm in the policy rollouts module at each episode is define as following,

$$\epsilon = \epsilon_e + (\epsilon_s - \epsilon_e) \cdot e^{-\frac{eps}{\epsilon_d}} \tag{29}$$

where ϵ_s and ϵ_e are the start and end values of the epsilon, ϵ_d refers to the epsilon decay rate, and eps represents current training episode index. Here, we set $\epsilon_s = 1$, $\epsilon_e = 0.01$, and $\epsilon_d = 200$. Then, the ϵ values over the whole training episodes are shown as Fig. 11. As the ϵ represents the probability of choosing random actions for exploration, the large value of ϵ, at the beginning stage of the training, encourages more explorations in the model training by generating random actions in the action space. As the training episode increases and more possible control policies the RDQN explored, the ϵ smoothly decay to small values, where the RDQN prefers to exploitations in the model training through generating actions by the trained control policy.

Moreover, to enhance the generalizability of the trained lane-change preclusion model, various lane-change scenarios and HDV driver types are considered in the RDQN model training. Specifically, for each training episode, the training environment will be randomly assigned with a lane-change scenario, as shown in Fig. 7, and a HDV driver type with driving behavior parameters from Tables 1 and 2. Then, the RDQN are trained of capability to handle different lane-change scenarios and HDV driver types. The scaling parameters in the MDP are determined based on a trial-and-error method to balance the trade-offs amongst all reward components in Equation (2), to achieve desired lane-change preclusion performance while retaining smoothness and safety. Finally, the cumulative reward effectively converges to around 1.14 within 1000 episodes of training, as shown in Fig. 12. The positive sign of the reward value indicates that the obtained optimal policy precludes undesired collision and reverse movements (otherwise, reward will be negative due to the significant penalty δ in the safety reward component in Equation (20)).

3.3 Results and discussion

We first examine the performance of the LTC-predictor in predicting the driving behavior of vehicle B and disruptive lane-change traffic conditions. Second, the effectiveness of the PLCS in precluding disruptive HDV lane changes, reducing oscillations, and improving traffic smoothness is evaluated in presence of different lane-change scenarios. Third, we conduct sensitivity analysis of the PLCS to investigate its effectiveness under different HDV driver types and CV control setups. Fourth, the performance of the time headway transition function is evaluated in smoothening control transition from the lane-change preclusion model to the car-following control model and reducing oscillations in lane-change preclusion failure cases. Finally, comprehensive discussions of the PLCS performance and its key limitations are provided.

3.3.1 Performance of LTC-predictor

Mean-square-error (MSE) is used as the performance metric for the LTC-predictor in terms of predicting driving behaviors of vehicle B and disruptive lane-change traffic conditions. The MSE between the predicted accelerations and the ground-truth accelerations of vehicle B across all testing data is 1.7e-06. The MSE between the predicted occurrences of disruptive lane-change conditions and the indications of ground-truth lane changes from MOBIL over all testing data is 4.8e-03. These results illustrate the robustness of the LTC-predictor.

3.3.2 Performance of PLCS

Three measurement metrics are introduced to examine the effectiveness of the PLCS under lane-change preclusion: (i) lane-change rate of vehicle B (denoted as CR here), which is the ratio of the number of experiments with lane change occurrence to the total number of experiments; (ii) variance of speed (VS) of the ego vehicle over the experiment duration k_{total}: $VS(v(k)) = (\sum_{k=0}^{k_{total}}(v(k) - \bar{v})^2)/k_{total}$; and (iii) fluctuation of acceleration (FA) of the ego vehicle: $FA(a(k)) = (\sum_{k=0}^{k_{total}}(a(k) - a(k-1))^2)/k_{total}$, where $v(k)$ and $a(k)$ are longitudinal speed and acceleration of the ego vehicle at time k, respectively. $\bar{v}$ is the mean longitudinal speed of the ego vehicle. k_{total} refers to the time duration of the experiment.

The PLCS is applied in both lane-change scenarios. Then, controlled experiments using the baseline strategy (i.e., the ego vehicle is controlled only by the EIDM-based car-following control model) are conducted and the results are used for comparison. Each strategy is executed over 1000 times in each scenario. In the experiments, the CV control setup of the ego vehicle is set as EIDM2, and vehicle B is assumed to be of the normal driver type. In scenario 1, the baseline strategy induces 87.4% HDV lane changes (i.e., CR of 87.4%) with VS of 8.2931 and FA of 1.2456, on average, while the PLCS induces 43.4% HDV lane changes with VS of 5.0911 and FA of 0.1936, on average. In scenario 2, the baseline strategy induces 86.5% HDV lane changes with VS of 5.8768 and FA of 0.8061, on average, while the PLCS induces 14.4% HDV lane changes with VS of 1.8674 and FA of 0.0792, on average. The results indicate that in both scenarios the PLCS is effective in precluding disruptive lane changes and thus improves traffic smoothness.

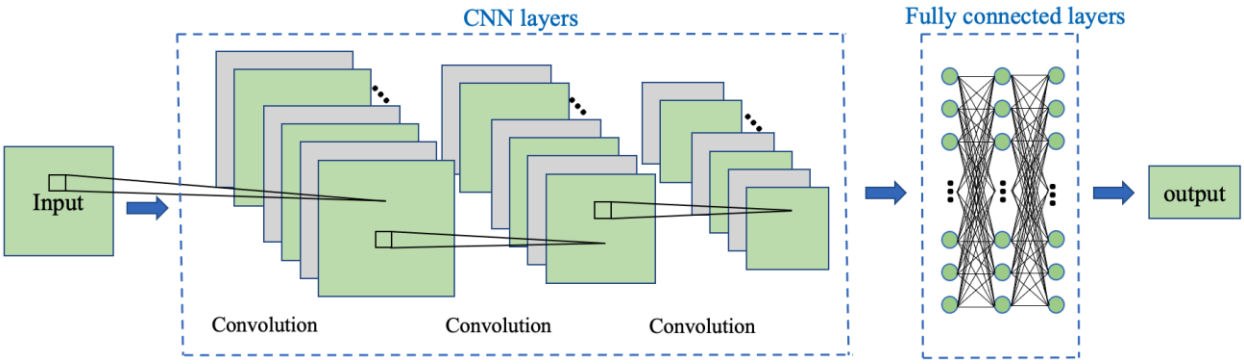

Figure 10. The RDQN architecture

Table 4. Parameters of lane-change preclusion model

MDP		RDQN	
$\boldsymbol{\theta_l}$	0.5	Learning rate	0.0001
$\boldsymbol{\theta_s}$	1	Episode number	1000
$\boldsymbol{\theta_a}$	0.1	Discount factor	0.95
$\boldsymbol{\theta_v}$	1	Batch size	5120
$\boldsymbol{\delta}$	10	Target update rate	10
$\boldsymbol{U}$	$\{-\mathbf{2.00}, -\mathbf{1.99}, \ldots, \mathbf{1.99}, \mathbf{2.00}\}$		

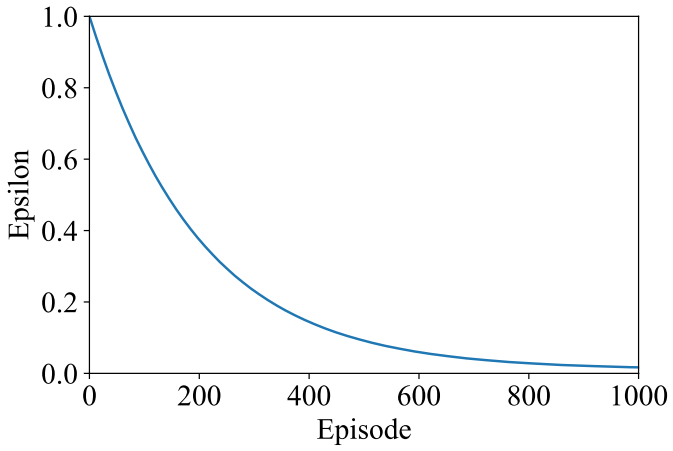

Figure 11. Epsilon greedy decay.

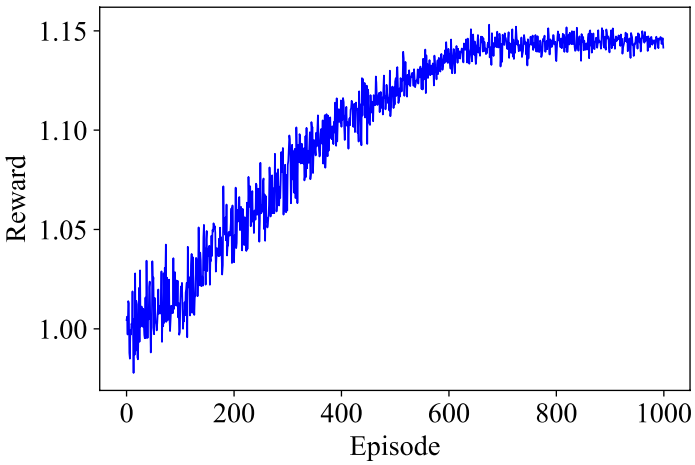

Figure 12. Reward convergence of RDQN training.

To further illustrate the performance differences between the PLCS and the baseline strategy, speed, and acceleration profiles of typical cases in the experiments are illustrated in Figs. 13 and 14 for the two scenarios.

The vertical dashed line represents the time at which the LTC-predictor indicates a disruptive lane-change traffic condition. For the baseline strategy, due to the large spacing between vehicle E and the ego vehicle caused by either the speeding behavior of vehicle E in scenario 1 or the cut-out of vehicle G in scenario 2, a disruptive lane change occurs by vehicle B from lane 2 to lane 1 (dash-dotted lines in Figs. 13(a), 13(c), 14(a) and 14(c)).

This lane change causes abrupt braking by the ego vehicle and the following vehicle C (as shown in Figs. 13(a) and 14(a)), and significant speed fluctuation in the CV platoon as shown in Figs. 13(c) and 14(c). In contrast, as shown in Figs. 13(b), 13(d), 14(b), and 14(d), using the PLCS, the ego vehicle successfully precludes the potential lane change by vehicle B (improving the CV platoon smoothness) and then smoothly switches back to car-following behavior without generating additional oscillations. Hence, the PLCS can deal with disruptive HDV lane changes under different lane-change scenarios. Thereby, it successfully precludes disruptive lane changes, reduces oscillations, and improves traffic smoothness.

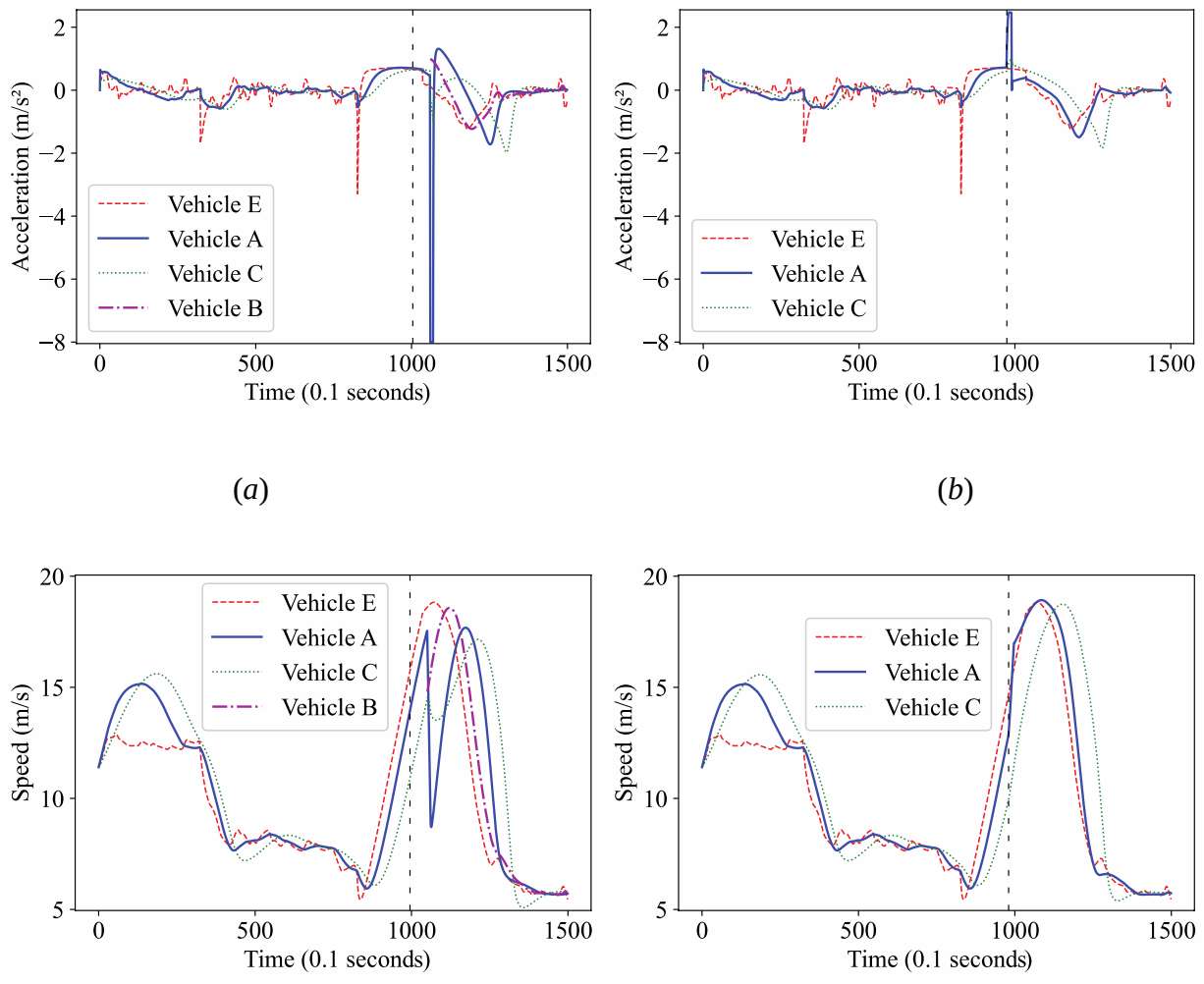

Figure 13. Performance comparison under scenario 1: (a) acceleration profile of baseline strategy, (b) acceleration profile of PLCS, (c) speed profile of baseline strategy, and (d) speed profile of PLCS

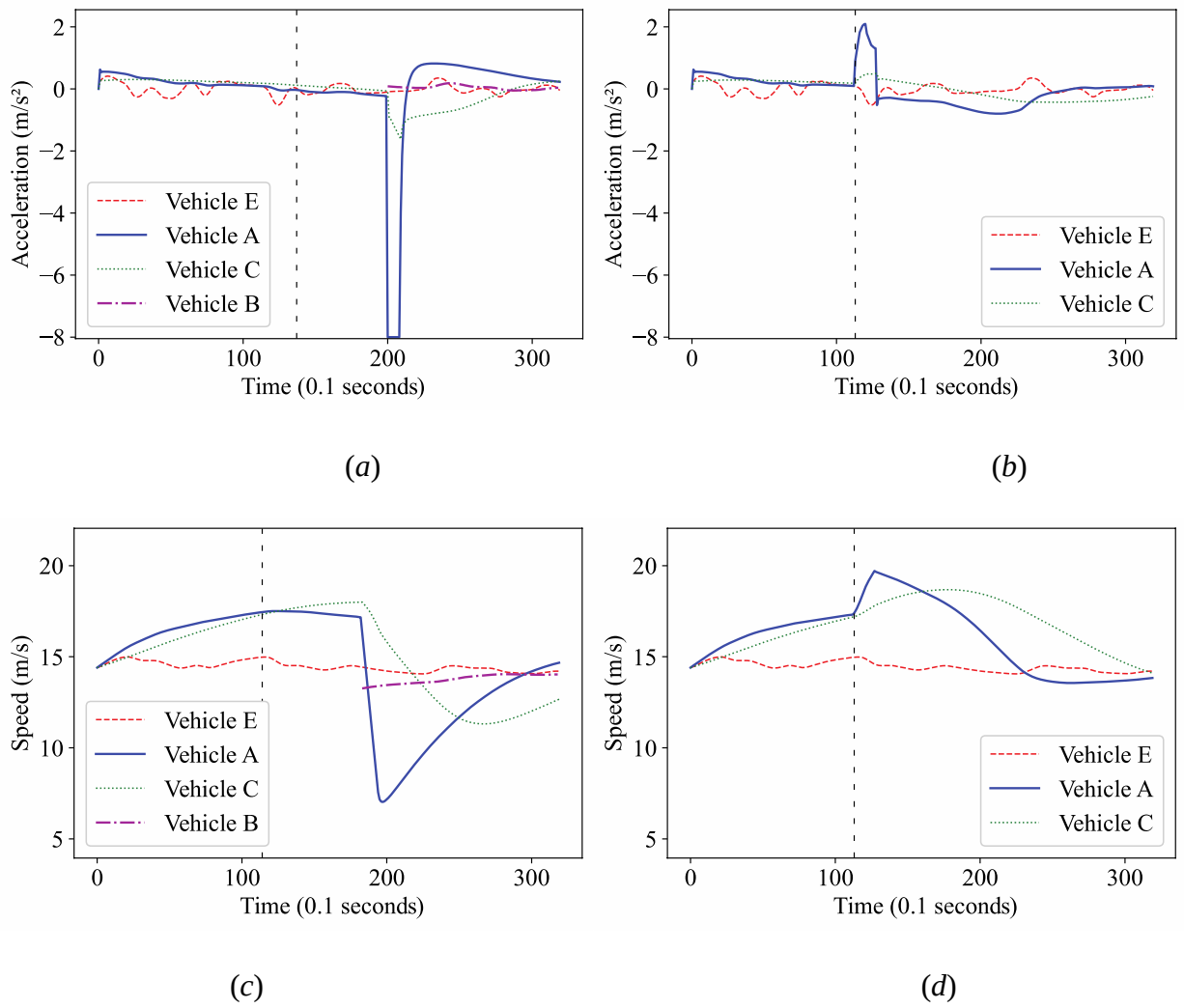

Figure 14. Performance comparison under scenario 2: (a) acceleration profile of baseline strategy, (b) acceleration profile of PLCS, (c) speed profile of baseline strategy, and (d) speed profile of PLCS.

3.3.3 Sensitivity analysis of PLCS

To examine the generalizability of the PLCS, experiments are conducted for the six lane-change cases shown in Table 5 consisting of various lane-change scenarios and HDV driver types. The corresponding parameter sets of the IDM and MOBIL are from Kesting et al. (2007) and Zhu et al. (2019), respectively, as shown previously in Tables 1 and 2. The experiments first seek to investigate the susceptibility of the ego vehicle in inducing lane changes by vehicle B. This is done by assuming that vehicle B will not execute any lane changes, and then comparing the lane-change time windows (i.e., the persisting time steps of continuous lane-change suggestions from MOBIL) in six cases, as shown in Table 6.

Table 6 shows that the PLCS has smaller lane-change time windows than that of the baseline strategy under all CV control setups. This suggests that it provides fewer lane-change opportunities to vehicle B. Table 7 shows that the PLCS has smaller CR values (i.e., lane-change rates) than the baseline strategy, illustrating its effectiveness in precluding more disruptive lane changes by vehicle B in all cases. The successful lane-change preclusion can be observed from the speed profiles in Figs. 15(b), 15(d), and 16(d). However, the PLCS fails to preclude lane change by vehicle B in Fig. 15(f), where the ego vehicle is controlled under EIDM3. This is because EIDM3 ensures the CV's string stability by maintaining a larger spacing with the preceding vehicle. The large spacing induces vehicle B to conduct a disruptive lane change more easily, while increasing the difficulty of preclusion. In addition, the PLCS fails when the HDV driver is aggressive, as shown in Fig. 16(b). In summary, the PLCS can successfully preclude disruptive HDV lane changes in most scenarios. However, a CV control setup for string stability (i.e., EIDM3) or aggressive HDV drivers can limit its ability for preclusion.

Table 5. Lane-change cases in experiments

Case	Lane-change scenario	HDV driver type
1	Scenario 1	Aggressive
2	Scenario 1	Normal
3	Scenario 1	Cautious
4	Scenario 2	Aggressive
5	Scenario 2	Normal
6	Scenario 2	Cautious

Table 6. Lane-change time window

Lane-change time window		Case					
		1	2	3	4	5	6
EIDM1	Baseline	22.189	14.649	7.464	39.631	23.014	6.658
	PLCS	14.595	8.269	4.56	19.461	6.975	2.25
EIDM2	Baseline	29.759	21.457	14.161	45.15	30.1	12.519
	PLCS	18.664	11.546	8.19	22.273	9.231	4.691
EIDM3	Baseline	72.327	59.564	48.757	88.392	71.544	49.865
	PLCS	39.646	27.442	22.882	35.528	17.951	11.982

Table 7. Lane-change rate

CR		Case					
		1	2	3	4	5	6
EIDM1	Baseline	89.80%	64.70%	6.10%	99.80%	72.10%	16.50%
	PLCS	61.20%	0.00%	0.00%	91.40%	6.60%	0.10%
EIDM2	Baseline	98.90%	87.40%	49.80%	99.80%	86.50%	42.00%
	PLCS	90.90%	43.40%	0.10%	99.30%	14.40%	1.30%
EIDM3	Baseline	100.00%	100.00%	100.00%	100.00%	100.00%	99.90%
	PLCS	100.00%	93.80%	96.20%	100.00%	36.60%	17.90%

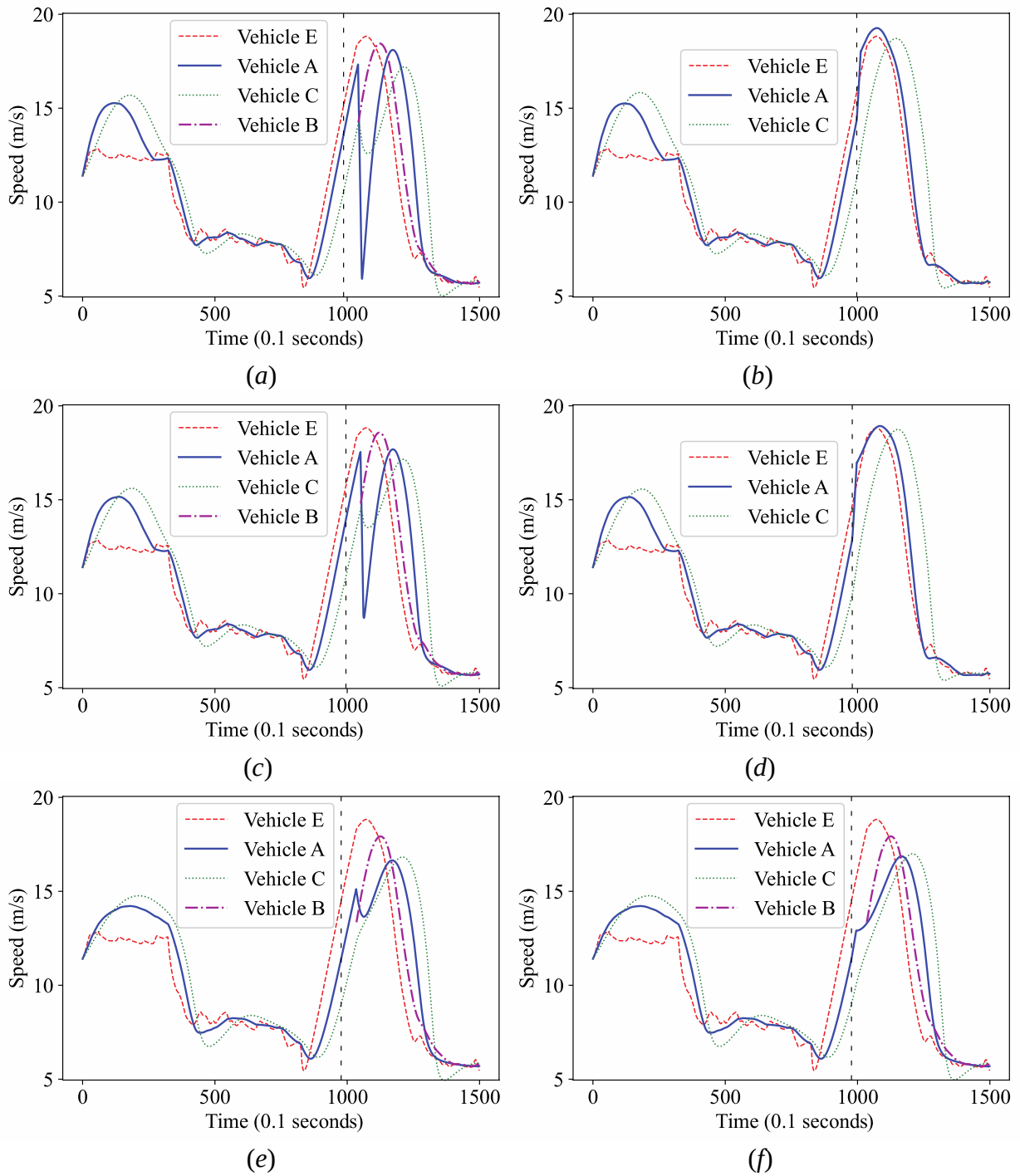

Figure 15. Speed profile in scenario 1 with normal HDV driver: (a) baseline strategy of EIDM1, (b) PLCS of EIDM1, (c) baseline strategy of EIDM2, (d) PLCS of EIDM2, (e) baseline strategy of EIDM3, and (f) PLCS of EIDM3.

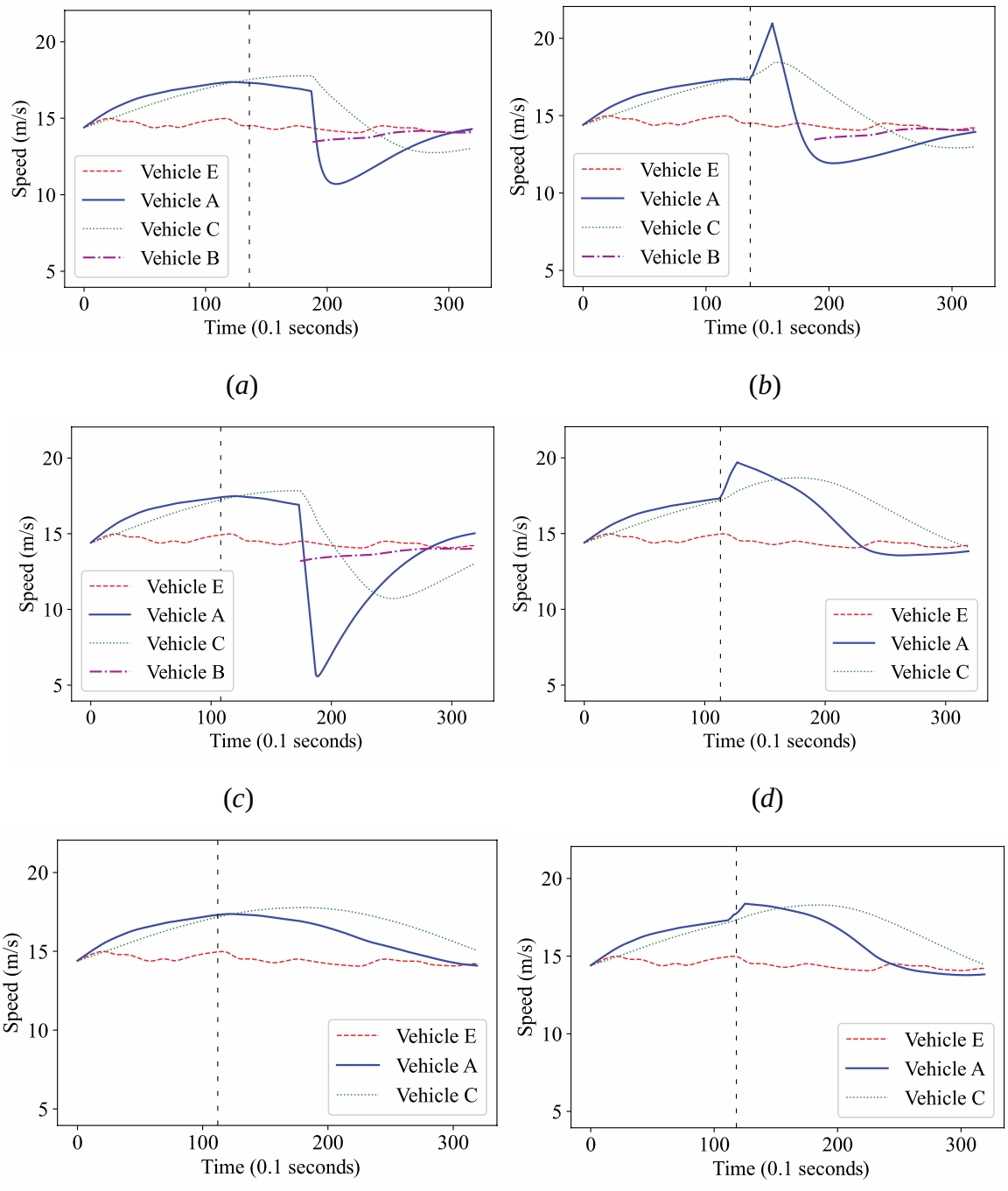

Figure 16. Speed profile in scenario 2 with CV control setup of EIDM1: (a) baseline strategy of aggressive HDV, (b) PLCS of aggressive HDV, (c) baseline strategy of normal HDV, (d) PLCS of normal HDV, (e) baseline strategy of cautious HDV, and (f) PLCS of cautious HDV.

Tables 8 and 9 illustrate that the PLCS generates smaller VS and FA values than those of the baseline strategy in most cases. It also causes fewer speed fluctuations for the ego vehicle than the baseline strategy, as illustrated by the speed profiles of Figs. 15 and 16. The ego vehicle controlled by the PLCS performs better than the baseline strategy in terms of reducing oscillations and improving smoothness in most cases. But, in some special cases, e.g., a CV control setup of EIDM3 or aggressive HDV drivers, the PLCS generates larger VS and FA values than those of the baseline strategy. These additional oscillations are caused by the lane-change preclusion failures, where the ego vehicle performs accelerations during the lane-change preclusion and abruptly switch to decelerations in the car-following control model to maintain safety. In summary, in most scenarios, the PLCS is effective in dealing with disruptive HDV lane changes, reducing oscillations, and improving traffic smoothness under various lane-change scenarios, CV control setups, and HDV driver types. But a CV control setup for string stability (i.e., EIDM3) or aggressive HDV drivers can limit its performance in traffic smoothness.

Tables 7, 8, and 9 illustrate CR, VS, and FA, respectively, when vehicle B executes lane changes. Note that results of Tables 6, 7, 8, and 9 are mean values over 1000 runs of experiments. Fig. 15 shows the speed profiles of the two control strategies in scenario 1 for a normal HDV driver and the three CV control setups (i.e., EIDM1, EIDM2, and EIDM 3). Fig. 16 illustrates the speed profiles of the two control strategies in scenario 2 for the three HDV driver types and the CV control setup of EIDM1.

Table 8. Variance of speed

VS		**Case**					
		1	2	3	4	5	6
EIDM1	Baseline	7.8365	7.2872	6.4846	1.8577	5.0661	0.9408
	PLCS	5.1127	6.2468	5.8407	4.9024	1.1914	0.2532
EIDM2	Baseline	6.0492	8.2931	6.5887	1.4276	5.8768	2.2090
	PLCS	3.5119	5.0911	6.1183	4.3680	1.8674	0.4992
EIDM3	Baseline	4.5233	2.4324	2.0840	0.0759	0.9809	4.0715
	PLCS	5.1098	3.1181	2.3470	2.2990	4.1020	3.0497

Table 9. Fluctuation of acceleration

FA		Case					
		1	2	3	4	5	6
EIDM1	Baseline	1.1875	0.8355	0.0549	0.5442	0.6782	0.1345
	PLCS	0.3963	0.0457	0.0388	0.3095	0.0641	0.0174
EIDM2	Baseline	1.0845	1.2456	0.5601	0.4614	0.8061	0.3258
	PLCS	0.3176	0.1936	0.0452	0.2374	0.0792	0.0259
EIDM3	Baseline	0.0111	0.0946	0.3615	0.0051	0.1533	0.6015
	PLCS	0.0777	0.0962	0.0942	0.0926	0.1481	0.1418

3.3.4 Performance of time headway transition function

The failure of lane-change preclusion can induce additional oscillations during the lane change maneuver of vehicle B (as shown in the non-smooth speed profiles in Figs. 15(f) and 16(b)). Due to the abrupt acceleration and high speed of the ego vehicle during lane-change preclusion and the small spacing between the ego vehicle and vehicle B after preclusion, the car-following control model of the PLCS can cause significant decelerations in the ego vehicle after the failure of the lane-change preclusion than under the baseline strategy. The time headway transition function described in Section 3.4 is used to handle this problem.

To analyze the effectiveness of the time headway transition function, the performance of the baseline strategy and the PLCS are compared with and without the time headway transition function. To simplify the comparison and focus on the effect of the transition function, only one example is presented, which is constructed based on both lane-change scenarios, EIDM2 CV control setup, and aggressive HDV driver type. Speed profiles of this example are shown in Figs. 17 and 18. Figs. 17(c), 17(d), 18(c), and 18(d) illustrate that the ego vehicle controlled by the PLCS without time headway transition generates substantial decelerations after the failure of the lane-change preclusion. By contrast, Figs. 17(e), 17(f), 18(e), and 18(f) show that the time headway transition function in the PLCS successfully alleviates abrupt decelerations by the ego vehicle, reduces additional oscillations, and ensures smooth platoon operation. Further, the failure of lane-change preclusion leads to degraded performance under the PLCS in some lane-change cases, as shown in Figs. 18(a), 18(b), 18(e), and 18(f). However, the time headway transition function enables the PLCS to perform smoother in other lane-change preclusion failure cases, as shown in Figs. 17(a), 17(b), 17(e), and 17(f).

In summary, the results indicate that the proposed time headway transition function can enable smooth control transition from the lane-change preclusion model to the car-following control model, and better manage situations with lane-change preclusion failures.

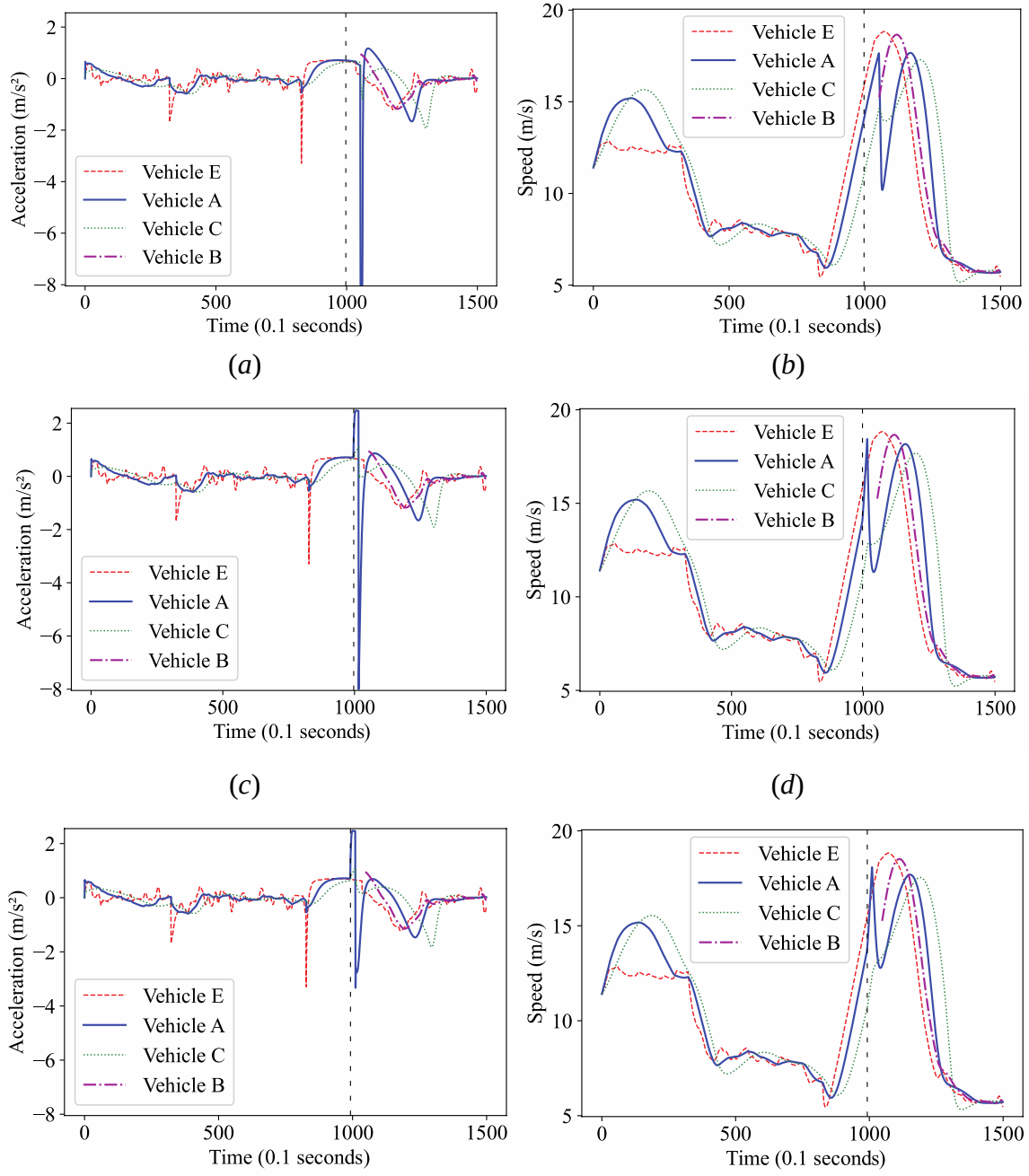

Figure 17. Performance comparison under lane-change preclusion failure in scenario 1: (a) acceleration profile of baseline strategy, (b) speed profile of baseline strategy, (c) acceleration profile of PLCS without time headway transition, (d) speed profile of PLCS without time headway transition, (e) acceleration profile of PLCS, and (f) speed profile of PLCS.

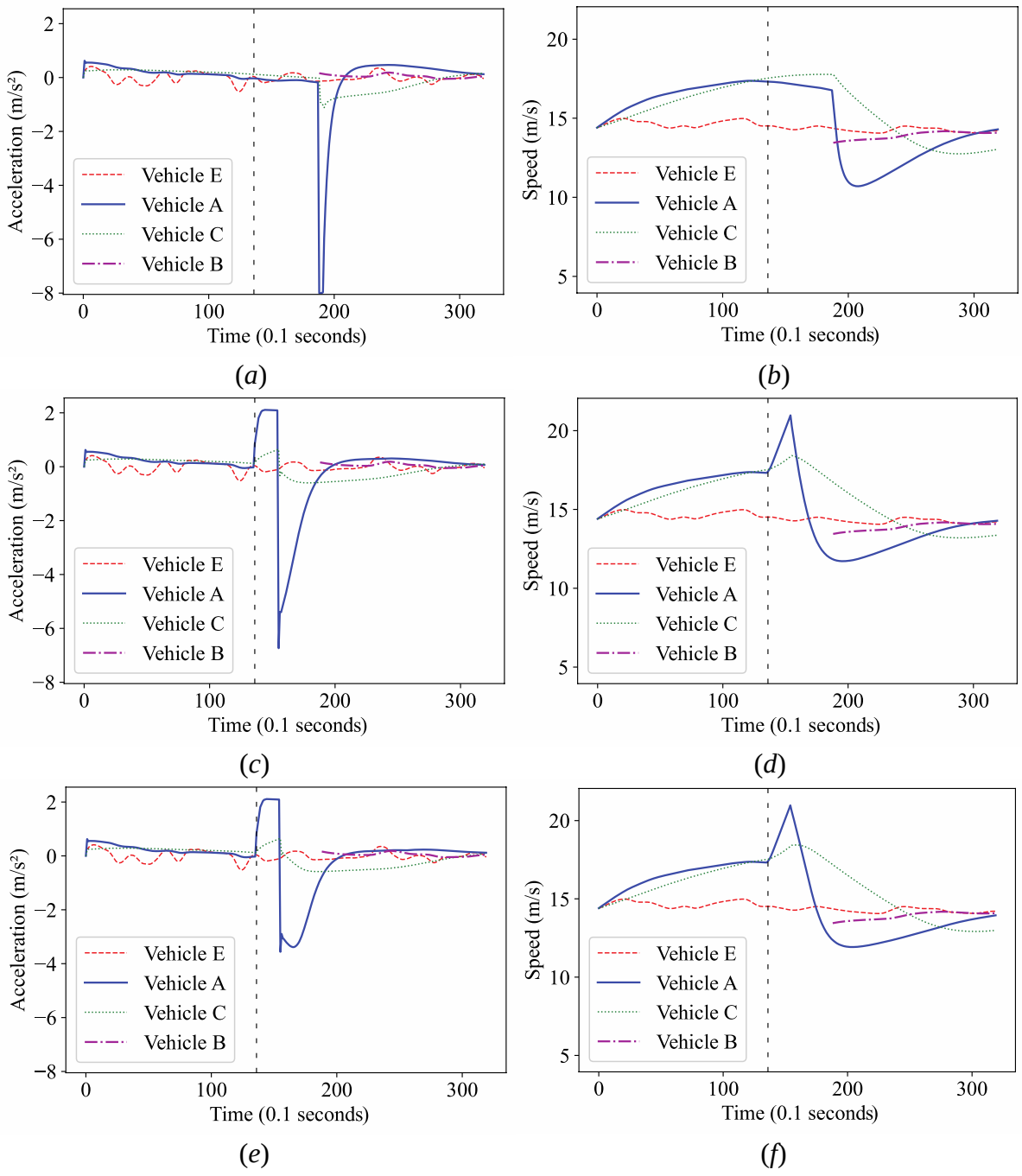

Figure 18. Performance comparison under lane-change preclusion failure in scenario 2: (a) acceleration profile of baseline strategy, (b) speed profile of baseline strategy, (c) acceleration profile of PLCS without time headway transition, (d) speed profile of PLCS without time headway transition, (e) acceleration profile of PLCS, and (f) speed profile of PLCS.

3.3.5 Discussions and limitations

The experiments in this section have examined the performance of the PLCS under different lane-change scenarios, CV control setups, and HDV driver types. Results in Tables 6 and 7 demonstrate that the PLCS provides fewer lane-change opportunities to vehicle B and preclude more disruptive HDV lane changes than the baseline strategy. However, as shown in Table 7, the PLCS does not successfully preclude all disruptive lane changes, and it fails in some situations with the CV control setup for string stability (i.e., EIDM3) or aggressive HDV drivers. This is consistent with the fundamental mechanism and control framework of the PLCS. The PLCS is not designed to directly block the lateral lane-change maneuver by vehicle B, but proactively preclude the potential disruptive lane change before vehicle B initiates the lane-change maneuver. To avoid unsafe CV-HDV interactions and maintain safety, it will automatically stop the lane-change preclusion process and let vehicle B cut in, if the ego vehicle observes the lane-change maneuver performed by vehicle B. In situations with large spacing setup (i.e., EIDM3) or aggressive HDV drivers, it is of challenge for the ego vehicle to preclude the disruptive lane change by vehicle B given a short response time (i.e., 1.5 seconds in the experiment, based on Finnegan & Green (1990)) before vehicle B perform lane-change maneuvers. Thus, the PLCS is still effective in precluding disruptive HDV lane changes in a safe manner in most situations.

In addition, results in Tables 8 and 9 demonstrate that the PLCS can enhance traffic smoothness in most cases. However, in some special lane-change failure cases, the PLCS still generate more oscillations than the baseline strategy even with the enhancement of the time headway transition function. This is the key limitation of the PLCS, that is, precluding disruptive lane changes does not always improve traffic smoothness in all situations. Instead, in some situations, e.g., aggressive HDV drivers, assisting lane changes might be a better choice. For future research, it is suggested to develop a proactive lane-change assistance control strategy to complement the PLCS in managing disruptive HDV lane changes. However, considering only the lane-change preclusion strategy domain, the PLCS successfully balance the trade-off between traffic efficiency and safety, and in most scenarios, it is effective in precluding disruptive HDV lane change, reducing oscillations, and improving traffic smoothness under various lane-change scenarios, CV control setups, and HDV driver types.

4. CONCLUDING COMMENTS

This paper proposes a deep reinforcement learning-based proactive longitudinal control strategy (PLCS) for CVs to preclude disruptive lane changes by HDVs, reduce oscillations, and improve string stability of the CV platoons. To the best of the authors' knowledge, this is the first study to investigate proactive preclusion of HDV lane changes by leveraging lane-change-related traffic information obtained by CVs and real-time CV-HDV interactions to foster traffic smoothness. The PLCS includes four components: Transformer-based LTC-predictor, EIDM-based car-following control model, RDQN-based lane-change preclusion model, and time headway transition function. When the Transformer-based LTC-predictor indicates a lane-change traffic condition, implying the potential for disruptive lane change by the HDV in adjacent lane, the RDQN-based lane-change preclusion model takes over and controls the CV to preclude disruptive lane changes. When no disruptive lane-change traffic condition is indicated by the LTC-predictor, the CV switches to the EIDM-based car-following control model and performs smooth car-following behavior under cooperative platooning control. A time headway transition function is proposed to smoothen the control transition from the lane-change preclusion model to the car-following control model, which prevents the ego vehicle from causing additional oscillations in lane-change preclusion failure cases. Results from numerical experiments indicate that the PLCS is effective in precluding disruptive HDV lane changes in mixed-flow traffic and improving CV platoon smoothness. The sensitivity analysis illustrates the generalizability of the PLCS under different lane-change scenarios, CV control setups, and HDV driver types.

The PLCS is designed to preclude disruptive HDV lane changes to reduce their adverse impacts on CV platoons. However, in some situations, e.g., a lane-merging scenario caused by an accident and mandatory lane changes exist, precluding disruptive lane changes can deteriorate the traffic performance and the CV need to assist HDV lane changes while maintaining safety and traffic smoothness. A future research direction is to develop proactive control strategies for CVs to manage HDV lane changes while seeking to balance lane-change preclusion and lane-change assistance objectives. Another research direction is to use a driving simulator environment to analyze the performance of the PLCS under mixed-flow traffic environments while eliciting real-world driver behaviors. Further, the PLCS focuses on controlling a CV in a lane-change scenario involving a single HDV lane change. It can be extended to a multi-agent cooperative lane-change management control strategy in multi-lane-change scenarios.

5. OUTPUTS, OUTCOMES, AND IMPACTS

5.1 List of research outputs (publications, conference papers, and presentations)

- Zhou, A., & Peeta, S. (2021). Cooperative Driving in Mixed-flow Traffic of Connected Vehicles and Human-driven Vehicles: A State Estimation Approach [Poster presentation]. *In 100th Annual Meeting of the Transportation Research Board*.

- Liu, Y., Zhou, A., Wang, Y., & Peeta, S. (2021). Proactive Longitudinal Control to Manage Disruptive Lane Changes of Human-Driven Vehicles in Mixed-Flow Traffic [Paper presentation]. *IFAC-PapersOnLin*e, 54(2), 321-326.

- Liu, Y., Zhou, A., Wang, Y., & Peeta, S. (2021, September). Proactive Longitudinal Control of Connected and Autonomous Vehicles with Lane-Change Assistance for Human-Driven Vehicles [Paper presentation]. *In 2021 IEEE International Intelligent Transportation Systems Conference (ITSC)* (pp. 776-781). IEEE.

- Liu, Y., Zhou, A., Wang, Y., & Peeta, S. (2022). Proactive Longitudinal Control to Manage Disruptive Lane Changes of Human-Driven Vehicles in Mixed-Flow Traffic [Poster presentation]. *In 101st Annual Meeting of the Transportation Research Board*.

- Liu, Y., Zhou, A., Wang, Y., & Peeta, S. (2022). Proactive Longitudinal Control of Connected and Autonomous Vehicles with Lane-Change Assistance for Human-Driven Vehicles [Poster presentation]. *In 101st Annual Meeting of the Transportation Research Board*.

5.2 Outcomes

This research project investigates the CV car-following mechanism in mixed-flow traffic and addresses the adverse impacts from lane changes by HDVs in adjacent lanes. Thereby, the proposed study will enhance the effectiveness and reliability of CV platooning operations in mixed-flow traffic environment. Besides, this project extends existing cooperative platooning control to multi-lane scenarios by successfully handle HDV lane-change challenges in mixed-flow traffic, such that the desired platoon control performance can be achieved to improve traffic flow.

5.3 Impacts

Connected vehicles (CV) technologies have the potential to help drivers make safe, reliable, and informed decisions, and thereby to enhance network capacity and reduce congestion. This project investigates a CV car-following model to reveal the CV movement characteristics during CV-HDV interactions and generate realistic CV trajectories in mixed flow environments. From the perspective of

transportation operation, the research outcomes shed lights on the future development CV platoon control to benefit the traffic flow in mixed-flow traffic. From the perspective of human quality-of-life and environment, the platoon control methods proposed in this project help enhance traffic safety, improve traffic efficiency, and reduce traffic oscillation.

5.4 Tech Transfer

In the execution of the project titled non-connected vehicle detection using connected vehicles – Phase 2, the research team undertook several technology transfer activities. The team gave three presentations at the TRB annual meeting, a conference with over 14,000 attendees; one presentation at the IFAC CTS conference; and one presentation at the IEEE International Conference on Intelligent Transportation Systems. The list below summarizes the tech transfer activities undertaken by the research team through the course of this project:

In 2021:

1. Conference presentation at the 100th Annual Meeting of the Transportation Research Board, Washington, D.C., USA: Cooperative Adaptive Cruise Control for Connected Autonomous Vehicles by Factoring Communication-Related Constraints, Wang, C., Gong, S. and Peeta, S. (2021).

2. Conference presentation at the 16th IFAC symposium on control in transportation systems, Lille, France: Proactive Longitudinal Control to Manage Disruptive Lane Changes of Human-Driven Vehicles in Mixed-Flow Traffic, Liu, Y., Zhou, A., Wang, Y., and Peeta, S. (2021).

3. Conference presentation at the 24th IEEE International Conference on Intelligent Transportation Systems, Indianapolis, IN, USA: Proactive Longitudinal Control of Connected and Autonomous Vehicles with Lane-Change Assistance for Human-Driven Vehicles, Liu, Y., Zhou, A., Wang, Y., and Peeta, S. (2021).

In 2022:

1. Conference presentation at the 101st Annual Meeting of the Transportation Research Board, Washington, D.C., USA: Proactive Longitudinal Control to Manage Disruptive Lane Changes of Human-Driven Vehicles in Mixed-Flow Traffic, Liu, Y., Zhou, A., Wang, Y., and Peeta, S. (2022).

2. Conference presentation at the 101st Annual Meeting of the Transportation Research Board, Washington, D.C., USA: Proactive Longitudinal Control of Connected and Autonomous Vehicles with Lane-Change Assistance for Human-Driven Vehicles, Liu, Y., Zhou, A., Wang, Y., and Peeta, S. (2022).

6. REFERENCES

Alexiadis, V., Colyar, J., Halkias, J., Hranac, R., & McHale, G. (2004). The next generation simulation program. *ITE Journal (Institute of Transportation Engineers)*, *74*(8), 22–26.

Altman, N. S. (1992). An introduction to kernel and nearest-neighbor nonparametric regression. *American Statistician*, 46(3), 175–185. https://doi.org/10.1080/00031305.1992.10475879

Bang, S., & Ahn, S. (2018). Control of connected and autonomous vehicles with cut-in movement using spring mass damper system. *Transportation Research Record*, *2672*(20), 133–143. https://doi.org/10.1177/0361198118796927

Basiri, M. H., Ghojogh, B., Azad, N. L., Fischmeister, S., Karray, F., & Crowley, M. (2020). Distributed nonlinear model predictive control and metric learning for heterogeneous vehicle platooning with cut-in/cut-out maneuvers. In *In 2020 59th IEEE Conference on Decision and Control (CDC)* (pp. 2849–2856).

Bellman, R. (1957). A Markovian decision process. *Indiana University Mathematics Journal*, *6*(4), 679–684. https://doi.org/10.1512/iumj.1957.6.56038

Bevly, D., Cao, X., Gordon, M., Ozbilgin, G., Kari, D., Nelson, B., Woodruff, J., Barth, M., Murray, C., Kurt, A., Redmill, K., & Ozguner, U. (2016). Lane change and merge maneuvers for connected and automated vehicles: a survey. *IEEE Transactions on Intelligent Vehicles*, *1*(1), 105–120. https://doi.org/10.1109/TIV.2015.2503342

Feng, S., Zhang, Y., Li, S. E., Cao, Z., Liu, H. X., & Li, L. (2019). String stability for vehicular platoon control: Definitions and analysis methods. *Annual Reviews in Control*, *47*, 81-97.

Finnegan, P., & Green, P. (1990). Time to change lanes: A literature review. *In the Annual Meeting of the Transportation Research Board, Washington, D.C.*

Fitch, G. M., Lee, S. E., Klauer, S., Hankey, J., Sudweeks, J., & Dingus, T. (2009). Analysis of lane-change crashes and near-crashes. *Final Report DOT HS 811 147, US Department of Transportation, National Highway Traffic Safety Administration*.

Hessel, M., Modayil, J., van Hasselt, H., Schaul, T., Ostrovski, G., Dabney, W., Horgan, D., Piot, B., Azar, M., & Silver, D. (2018). Rainbow: combining improvements in deep reinforcement learning. *32nd AAAI Conference on Artificial Intelligence, AAAI 2018*.

Izquierdo, R., Quintanar, A., Parra, I., Fernandez-Llorca, D., & Sotelo, M. A. (2019). Experimental validation of lane-change intention prediction methodologies based on CNN and LSTM. *2019 IEEE Intelligent Transportation Systems Conference, ITSC 2019*, 3657–3662. https://doi.org/10.1109/ITSC.2019.8917331

Jia, B., Yang, D., Zhang, X., Wu, Y. and Guo, Q. (2020). Car-following model considering the lane-changing prevention effect and its stability analysis. *The European Physical Journal B*, 93(8),1-9.

Jia, D., Lu, K., Wang, J., Zhang, X., & Shen, X. (2016). A survey on platoon-based vehicular cyber-physical systems. *IEEE Communications Surveys and Tutorials*, *18*(1), 263–284.

https://doi.org/10.1109/COMST.2015.2410831
Jin, W. L. (2010). Macroscopic characteristics of lane-changing traffic. *Transportation Research Record*, *2188*(1), 55–63. https://doi.org/10.3141/2188-07
Kesting, A., Treiber, M., & Helbing, D. (2007). General lane-changing model MOBIL for car-following models. *Transportation Research Record*, *1999*(1), 86–94. https://doi.org/10.3141/1999-10
Lenz, D., Kessler, T., & Knoll, A. (2016). Tactical cooperative planning for autonomous highway driving using Monte-Carlo tree search. *IEEE Intelligent Vehicles Symposium, Proceedings*, *2016-August*. https://doi.org/10.1109/IVS.2016.7535424
Mahajan, V., Katrakazas, C., & Antoniou, C. (2020). Prediction of lane-changing maneuvers with automatic labeling and deep learning. *Transportation Research Record*, *2674*(7), 336–347. https://doi.org/10.1177/0361198120922210
Milanés, V., & Shladover, S. E. (2016). Handling cut-in vehicles in strings of cooperative adaptive cruise control vehicles. *Journal of Intelligent Transportation Systems: Technology, Planning, and Operations*, *20*(2), 178–191. https://doi.org/10.1080/15472450.2015.1016023
Milanes, V., Shladover, S. E., Spring, J., Nowakowski, C., Kawazoe, H., & Nakamura, M. (2014). Cooperative adaptive cruise control in real traffic situations. *IEEE Transactions on Intelligent Transportation Systems*, *15*(1). https://doi.org/10.1109/TITS.2013.2278494
Mnih, V., Kavukcuoglu, K., Silver, D., Graves, A., Antonoglou, I., Wierstra, D., & Riedmiller, M. (2013). Playing Atari with deep reinforcement learning. *ArXiv Preprint ArXiv:1312.5602*.
Pouyan, M., Mousavi, A., Golzari, S., & Hatam, A. (2014). Improving the performance of Q-learning using simultanouse Q-values updating. *In 2014 International Congress on Technology, Communication and Knowledge (ICTCK)* ,1-6.
Roncoli, C., Bekiaris-Liberis, N., & Papageorgiou, M. (2017). Lane-changing feedback control for efficient lane assignment at motorway bottlenecks. *Transportation Research Record*, *2625*(1), 20–31. https://doi.org/10.3141/2625-03
Schmidhuber, J. (2015). Deep learning in neural networks: an overview. In *Neural Networks* (Vol. 61, pp. 85–117). https://doi.org/10.1016/j.neunet.2014.09.003
Schulman, J., Wolski, F., Dhariwal, P., Radford, A., & Klimov, O. (2017). Proximal policy optimization algorithms. *arXiv preprint arXiv:1707.06347*.
Shladover, S. E., Su, D., & Lu, X. Y. (2012). Impacts of cooperative adaptive cruise control on freeway traffic flow. *Transportation Research Record*, *2324*. https://doi.org/10.3141/2324-08
Steven A. Smith. (1985). Freeway data collection for studying vehicle interactions *(No. FHWA-RD-85-108). United States. Federal Highway Administration.*
Sutton, R. S., & Barto, A. G. (2018). Reinforcement learning, second edition: an introduction. In *The MIT Press*. MIT press.
Treiber, M., Hennecke, A., & Helbing, D. (2000). Congested traffic states in empirical observations and microscopic simulations. *Physical Review E - Statistical Physics, Plasmas, Fluids, and Related Interdisciplinary Topics*, *62*(2), 1805–1824. https://doi.org/10.1103/PhysRevE.62.1805

van Arem, B., van Driel, C. J. G., & Visser, R. (2006). The impact of cooperative adaptive cruise control on traffic-flow characteristics. *IEEE Transactions on Intelligent Transportation Systems*, *7*(4), 429–436. https://doi.org/10.1109/TITS.2006.884615

Vaswani, A., Shazeer, N., Parmar, N., Uszkoreit, J., Jones, L., Gomez, A. N., Kaiser, Ł., & Polosukhin, I. (2017). Attention is all you need. *Advances in Neural Information Processing Systems*, *2017-December*.

Ward, J. A. (2009). Heterogeneity, lane-changing and instability in traffic: a mathematical approach. Doctoral dissertation, University of Bristol.

Watkins, C. J. C. H., & Dayan, P. (1992). Q-learning. *Machine Learning*, *8*(3–4). https://doi.org/10.1007/bf00992698

Wissing, C., Nattermann, T., Glander, K. H., & Bertram, T. (2017). Probabilistic time-to-lane-change prediction on highways. *IEEE Intelligent Vehicles Symposium, Proceedings*, 1452–1457. https://doi.org/10.1109/IVS.2017.7995914

Yao, S., Knoop, V. L., & van Arem, B. (2017). Optimizing traffic flow efficiency by controlling lane changes: collective, group, and user optima. *Transportation Research Record*, *2622*(1). https://doi.org/10.3141/2622-09

Yu, H., Tseng, H. E., & Langari, R. (2018). A human-like game theory-based controller for automatic lane changing. *Transportation Research Part C: Emerging Technologies*, *88*, 140–158. https://doi.org/10.1016/j.trc.2018.01.016

Zhao, X., He, R., & Wang, J. (2020). How do drivers respond to driving risk during car-following? Risk-response driver model and its application in human-like longitudinal control. *Accident Analysis and Prevention*, *148*. https://doi.org/10.1016/j.aap.2020.105783

Zheng, Z., Ahn, S., Chen, D., & Laval, J. (2011). Freeway traffic oscillations: microscopic analysis of formations and propagations using wavelet transform. *Transportation Research Part B: Methodological*, *45*(9), 1378–1388. https://doi.org/10.1016/j.trb.2011.05.012

Zhou, A., Gong, S., Wang, C., & Peeta, S. (2020). Smooth-switching control-based cooperative adaptive cruise control by considering dynamic information flow topology. *Transportation Research Record*, *2674*(4), 444–458. https://doi.org/10.1177/0361198120910734

Zhou, A. and Peeta, S. (2021). Cooperative driving in mixed-flow traffic of connected vehicles and human-driven vehicles: a state estimation approach. *In 100th Annual Meeting of the Transportation Research Board, Washington, D.C*. https://doi.org/10.13140/RG.2.2.24614.24643

Zhu, B., Jiang, Y., Zhao, J., He, R., Bian, N., & Deng, W. (2019). Typical-driving-style-oriented personalized adaptive cruise control design based on human driving data. *Transportation Research Part C: Emerging Technologies*, *100*, 274–288. https://doi.org/10.1016/j.trc.2019.01.025